

## SUBCLUSTERING IN RICH CLUSTERS OF GALAXIES AND THEIR ENVIRONS

MICHAEL J. WEST AND AUGUSTUS OEMLER, JR.  
 Department of Astronomy, Yale University

AND

AVISHAI DEKEL  
 Racah Institute of Physics, Hebrew University of Jerusalem  
 Received 1987 May 11; accepted 1987 September 24

### ABSTRACT

Rich clusters of galaxies and their environs are studied by comparing high-resolution  $N$ -body simulations with observations, to examine whether the degree of subclustering in and around clusters is sensitive to the cosmogonic scenario which led to their formation. If it is, this sensitivity could be used to help constrain the allowable initial density fluctuations from which the presently observed large-scale structure of the universe might have arisen. Several new statistical methods for measuring the degree of subclustering are presented. The amount of substructure within the main bodies of rich clusters is found to be not very sensitive to the initial conditions. In general, the observed subclustering is much weaker than has sometimes been claimed and is in many cases no larger than that expected from random fluctuations. This suggests that most rich clusters are in a relaxed state at present. Virial and projected mass estimates are also consistent with most rich clusters having already relaxed. A more promising means for distinguishing between the different cosmogonic scenarios is found from statistical measurements of small-scale clustering in the regions immediately surrounding rich clusters in the simulations, which show significant dependence on the amount of small-scale power present in the initial fluctuation spectrum. This suggests that observational studies of the small-scale clustering of galaxies in the regions surrounding rich clusters and in the field may provide perhaps the most promising means yet for distinguishing between different cosmogonies.

*Subject headings:* cosmology — galaxies: clustering — galaxies: formation

### I. INTRODUCTION

Most currently popular cosmogonic models assume that the early universe was essentially homogeneous except for the presence of small-amplitude density fluctuations, and that the growth of large-scale structure from these initial fluctuations can be understood in terms of gravitational instability in an expanding universe. However, because at present it is difficult to place strong constraints on the types of primordial perturbations, on the form of the initial fluctuation spectrum, or even on the dominant mass component of the universe, several very different though equally viable scenarios are possible within this gravitational instability framework. In the extremes, structure is believed to have formed either by clustering hierarchically from small to large scales (e.g., Peebles and Dicke 1968; White and Rees 1979) or via fragmentation from large to small scales (e.g., Zel'dovich 1970; Doroshkevich, Shandarin, and Saar 1978), depending on the exact form of the initial fluctuation spectrum. If primordial perturbations occurred in both the matter and radiation fields such that the baryon/photon ratio remained constant (i.e., adiabatic perturbations), then photon diffusion and viscosity prior to the onset of the gravitational instability era would have erased all density fluctuations below a characteristic comoving length of  $\sim 3(\Omega h^2)^{-3/4}$  Mpc (Silk 1968), resulting in the collapse of supercluster-sized pancakes which would subsequently fragment into clusters and galaxies (here and throughout,  $\Omega$  is the ratio of the present density of matter in the universe to the critical value required for closure and  $h$  is the Hubble constant in units of  $100 \text{ km s}^{-1} \text{ Mpc}^{-1}$ ). A similar pancake scenario would arise if neutrinos possessing a nonzero rest mass (say  $\sim 30 \text{ eV}$ ) are the dominant mass component of the universe, since free streaming of these particles

while still relativistic would have erased fluctuations below a comoving length  $\sim 41 m_{30} h^{-1}$  Mpc, where  $m_{30}$  is the neutrino mass in units of  $30 \text{ eV}$  (Bond, Efstathiou, and Silk 1980; Doroshkevich *et al.* 1981). If, on the other hand, the initial perturbations were such that the matter density was perturbed on top of a uniform radiation background (i.e., isothermal perturbations), then density fluctuations would have initially been present on all relevant scales. In this scenario, the formation of structure would proceed in a hierarchical manner, from galaxies, to clusters of galaxies, to superclusters. A similar hierarchical clustering scenario would also be expected if the universe is dominated by weakly interacting, nonbaryonic particles, or "cold dark matter" (e.g., Pagels and Primack 1982; Peebles 1982), although in this case the collapse of structure on different scales is expected to occur over a short cosmological time interval, since the predicted initial fluctuation spectrum is quite flat over a wide range. Hybrid scenarios are also possible, in which the initial fluctuation spectrum possesses a coherence length as in the neutrino scenario, but with an additional low-amplitude small-scale component. A fluctuation spectrum of this type might result from the presence of different types of dark matter or perturbations (e.g., Dekel 1983, 1984; Dekel and Aarseth 1984), or if the universe underwent more than one inflationary phase (Silk and Turner 1986; Turner *et al.* 1987).

As an attempt to confront the different theoretical scenarios with observations, rich clusters of galaxies have been studied here and in other papers (West, Dekel, and Oemler 1987*a*; West, Dekel, and Oemler 1987*b*; West, Oemler, and Dekel 1987; hereafter Papers I, III, and IV, respectively). Although clusters of galaxies are at a more advanced dynamical stage

than superclusters and voids, the hope is that some memory of the cosmological initial conditions has survived the cluster collapse and subsequent evolution. The principle advantage of studying rich clusters is that they are a well-studied class of objects, and as such there are at present many good data available for a large number of clusters. However, because clusters are very nonlinear systems at the present epoch, they are not amenable to analytic studies such as those used to describe the linear evolution of density fluctuations. Thus, one must resort to numerical simulations in order to extrapolate the evolution of structure from some assumed primordial linear fluctuation spectrum into the nonlinear regime. By comparing the systematic properties of clusters of galaxies formed in  $N$ -body simulations of different cosmological scenarios with observations of real clusters, it is hoped that it will be possible to constrain the range of viable scenarios.

One of the fundamental differences between the various cosmogonic scenarios is the presence, or lack, of a small-scale component in the primordial spectrum of density fluctuations. Because it is this component which is responsible for the formation of small-scale structure, one would expect the number and sizes of small groups and subclusters to be a tell-tale sign of the form of the initial power-spectrum. Thus a quantitative description of the degree of small-scale clustering, both within rich clusters and their environs, might provide a strong test of the different scenarios. This is rather different from the usual approach of searching for traces of the cosmological initial conditions using the largest scale structures, such as superclusters and voids. Nevertheless, any theoretical scenario which purports to describe the origin and evolution of the large-scale structure must also be able to explain the observed distribution of pairs and groups of galaxies. Furthermore, it must be able to account for the presence at the present epoch of both centrally concentrated, relaxed clusters like Coma, and very irregular, clumpy systems such as Hercules.

The presence, and degree, of substructure within clusters of galaxies may also provide valuable information on the dynamical states of clusters (White 1976; White and Rees 1979; Geller 1984; Cavaliere *et al.* 1986), as well as on the process of cluster formation itself. Violent relaxation associated with cluster collapse should destroy most subclustering within rich clusters, especially in their inner regions. Therefore, if most clusters do indeed possess a significant amount of substructure, then they are most probably still in the precollapse phase, and hence not yet relaxed systems. In this case, estimates of cluster masses from application of the virial theorem would be in error.

Unfortunately subclustering is notoriously difficult to measure in a meaningful, quantitative, and unambiguous way. The presence and significance of subclustering depends greatly on what criteria one chooses for identifying such structure. Numerous authors have claimed to detect substructure within clusters (e.g., Geller and Beers 1982; Gioia *et al.* 1982; Baier 1983, 1984, and references therein; Bothun *et al.* 1983; Quintana, de Souza, and Arakaki 1986; Fitchett and Webster 1986; Fabricant *et al.* 1986; Binggeli, Tammann, and Sandage 1987; Mellier *et al.* 1987). It has even been claimed that the oft-observed and enigmatic secondary maximum in the surface density profiles of clusters (e.g., Omer, Page, and Wilson 1965; Bahcall 1971; Austin and Peach 1974; Oemler 1974; Dressler 1978, 1980a) can be explained in terms of subclustering (Baier 1983; although see Bahcall 1971). X-ray observations also seem to suggest the presence of substructure in some clusters

(see, for example, Foreman and Jones 1982, and references therein). To date, the most thorough search for substructure has been that of Geller and Beers (1982). Using surface number density contour maps based on the galaxy positions given by Dressler (1976, 1980b) in his study of 65 rich clusters, they concluded that substructure is a common phenomenon in clusters, occurring in  $\sim 40\%$  of the clusters in the Dressler sample. Baier (1983) has suggested that perhaps as few as 20% of observed clusters can be considered real, single, relaxed systems, with most clusters being essentially agglomerations of smaller lumps.

To provide an objective measure of the presence and significance of subclustering three new statistical methods were devised and tested, and then applied to samples of both simulated and real clusters. The  $N$ -body cluster simulations used in this study are briefly described in § II. The statistical tests for subclustering are then described and applied to the simulated and observed clusters in § III. In § IV, small-scale clustering in the regions surrounding rich clusters is studied. Finally, § V contains a discussion of the results and conclusions.

## II. INITIAL CONDITIONS FOR $N$ -BODY SIMULATIONS

While numerous previous studies have been done using  $N$ -body simulations of different cosmogonic scenarios (e.g., Aarseth, Gott, and Turner 1979; Efstathiou and Eastwood 1981; Frenk, White, and Davis 1983; Miller 1983; Melott 1983; Centrella and Melott 1983; Klypin and Shandarin 1983; Dekel and Aarseth 1984; Dekel, West, and Aarseth 1984; Efstathiou *et al.* 1985; Davis *et al.* 1985; Frenk *et al.* 1986), resolution on the scale of clusters in these simulations has generally been too low for use in a detailed study of the systematic properties of clusters. This is because the dynamical range which it is possible to treat in such large-scale simulations is quite limited; one is attempting to model a large volume of the universe using a limited number of particles, consequently, each individual particle must be quite massive.

In order to simulate clusters with the desired high resolution, a novel approach was used here, in which the clusters were simulated in two steps. First, low-resolution, large-scale cosmological simulations of the different theoretical scenarios were performed to find the locations where proto-clusters formed for a given set of initial conditions. These results were then used to generate the initial conditions for the second, major step, in which high-resolution simulations of individual clusters were performed. In this way, it is possible to study in detail the properties of clusters formed from a wide range of cosmological initial conditions.

### a) General Method

A general method for generating any desired form of the initial fluctuation spectrum has been described in detail in Paper I, and is reviewed here only briefly. The objective is to represent the assumed power spectrum of small-density fluctuations at the onset of the gravitational instability era in each of the different cosmological scenarios being considered. It is assumed here that density perturbations in the early universe were Gaussian, so that the spatial fluctuations can be expressed in terms of Fourier components with random phases. The simplest form for such an initial fluctuation spectrum is a power law,

$$\langle |\delta_k|^2 \rangle \propto k^n \quad (1)$$

where  $\delta_k$  are Fourier components of the dimensionless density fluctuations  $\delta\rho/\rho$ . In this case, rms fluctuations on a given mass scale  $M$  in the linear regime vary as

$$\delta M/M \propto M^{-(3+n)/6}. \quad (2)$$

The task of generating the initial conditions for the  $N$ -body simulations then amounts to distributing a finite number of particles within the simulation volume in such a way that the desired initial power spectrum is accurately represented within some range of interest  $k_{\min} < k < k_{\max}$ . A convenient method for realizing the initial power spectrum is based on the approximation developed by Zel'dovich (1970) for describing the linear evolution of density fluctuations. In general, the Eulerian position,  $r$ , of any particle in an expanding cosmology at some time,  $t$ , can be expressed as a combination of its Lagrangian (comoving) position,  $q$ , and some displacement from that position. Zel'dovich showed that in the linear regime, one can conveniently approximate this displacement by assuming it to be composed of separate spatially dependent and temporally dependent terms. Specifically,

$$r = a(t)[q - b(t)\psi(q)], \quad (3)$$

where  $a(t)$  is the cosmological expansion factor [and hence  $a(t)q$  is the unperturbed position],  $b(t)$  is the growth rate of linear density fluctuations in the universe, and  $\psi(q)$  represents the spatial perturbation. For  $\Omega \sim 1$ ,  $b(t)$  scales linearly with the expansion factor  $a(t)$ . The question then is how to generate the spatial perturbation,  $\psi(q)$ , for the desired initial spectrum of density fluctuations. Briefly, since the perturbations are assumed to be uncorrelated,  $\psi(q)$  can be generated by the superposition of small-amplitude plane waves of random phases and directions. This procedure was implemented as follows.  $N$  particles were initially distributed uniformly inside a unit sphere of volume  $V$ . The particles were distributed at the points of a cubic grid, so as to initially suppress any undesired small-scale noise, with  $(V/N)^{1/3}$  grid points used. Then, the position of each particle (and in the pancake and hybrid scenarios, its velocity as well; see § IIb) was perturbed by a superposition of  $N_k$  small-amplitude sine waves with randomly chosen phases and directions. Using this procedure, the desired initial power spectrum should be faithfully represented on scales down to twice the initial separation of grid points. The evolution of each system in the linear regime was then followed using the Zel'dovich approximation until a stage where the rms density contrast on a comoving scale  $\lambda_u = 0.5$  (in units of the radius of the initial sphere size of the simulation) reached  $\sim 0.25$ . The cosmological expansion factor,  $a(t)$ , was then set equal to 1, and the  $N$ -body simulations begun. Again, the reader is referred to Paper I for further details.

#### b) Initial Conditions for Different Cosmogonic Scenarios

Simulations were performed for the following five scenarios: (a) a pancake scenario with a spectrum truncated above some critical wavenumber, (b) a hybrid scenario in which the initial perturbation spectrum possesses a coherence length as well as a small-scale component, and (c), (d), and (e) three hierarchical clustering scenarios with power-spectrum indices  $n = 0$ ,  $-1$ , and  $-2$ , respectively. All of these simulations assumed an Einstein-de Sitter universe ( $\Omega = 1$ ). However, the simulations done of the  $n = 0$  hierarchical clustering scenario were also repeated for an open universe,  $\Omega = 0.15$  at the present epoch. The specific initial conditions for each scenario are described below and summarized in Table 1.

TABLE 1  
PARAMETERS OF INITIAL FLUCTUATION SPECTRA<sup>a</sup>

Model	Scenario	$n$	$\lambda_{\min}^b$	$\lambda_u$	$\lambda_{\max}$	$\Omega$	$a_0^c$
a.....	Pancake	0	0.5	0.5	1.0	1	5.7
b.....	Hybrid <sup>d</sup>	0, 0	0.1, 0.5	0.5	0.5, 1.0	1	5.7
c.....	Hierarchical	0	0.1	0.5	1.0	1	11.3
d.....	Hierarchical	-1	0.075	0.5	1.0	1	11.3
e.....	Hierarchical	-2	0.075	0.5	1.0	1	11.3
f.....	Hierarchical	0	0.1	0.5	1.0	0.15	22.6

<sup>a</sup> For details see text.

<sup>b</sup> All wavelengths are in units of the radius of the initial sphere of the large-scale simulations.

<sup>c</sup> Expansion factor at which the clusters were studied.

<sup>d</sup> Amplitude jump at  $\lambda_u$  is a factor of 2 in  $|\delta_k|$ .

#### i) Pancake Scenario

Here the initial spectrum was truncated at a critical wavenumber,  $k_u$ , which should represent the coherence length expected to result from photon diffusion in adiabatic perturbations or the damping length in a neutrino-dominated universe. The form of the linear fluctuation spectrum was taken as

$$\langle \delta_k \rangle^2 \propto k^n \quad \text{for } k_{\min} < k < k_{\max}; \quad (4)$$

$$0 \quad \text{otherwise.}$$

A power-spectrum index  $n = 0$  was assumed.  $N_k = 200$  waves were used here, from  $k_{\min} = 2\pi$  until the spectrum was truncated at  $k_{\max} = 4\pi$ , corresponding to perturbations on scales  $\lambda_{\min} = 0.5$  to  $\lambda_{\max} = 1.0$  in units of the radius of the initial sphere size of the simulations. Thus, the coherence length in these simulations should result in the formation of pancakes whose comoving diameter is about one-half the simulation size. In addition to the density perturbations, perturbations to the velocity field were also included (as would be expected for adiabatic perturbations), with the peculiar velocity of each particle relative to the Hubble flow being given by the time derivative of equation (3).

#### ii) Hierarchical Clustering Scenarios

Here fluctuations were initially present on all scales. To examine the effects of having different amounts of power on large and small scales, simulations were performed for three different values of the power-spectrum index,  $n = 0$ ,  $-1$ , and  $-2$ .  $N_k = 700$  waves were used in all cases. For the case  $n = 0$ , the initial fluctuations ranged from  $\lambda_{\min} = 0.1$  to  $\lambda_{\max} = 1.0$ , while  $\lambda_{\min} = 0.075$  for  $n = -1$  and  $-2$ . In these simulations the particles had no initial peculiar velocities superposed on the general Hubble expansion. Simulations with identical initial conditions were run for the  $n = 0$  case in both flat and open universes. Although not explicitly simulated here, a cosmological scenario in which cold dark matter dominates is also essentially a sequence of hierarchical clustering. The primary difference between this scenario and the aforementioned hierarchical clustering scenario has to do with the form of the initial power spectrum. Specifically, the cold dark matter scenario predicts a well-defined shape of the initial fluctuation spectrum which cannot be represented by a single power law over a wide range of wavelengths. However, on the relevant scales for clusters of galaxies, the slope of the power spectrum in the cold dark matter scenario lies roughly between 0 and  $-1$ , and hence can be approximated by either the  $n = 0$  or  $n = -1$  hierarchical clustering cases studied here.

iii) *Hybrid Scenario*

To model this scenario, the large-scale component of the initial perturbation spectrum was truncated at a critical wavelength, with fluctuations present from  $\lambda_{\min} = 0.5$  to  $\lambda_{\max} = 1.0$ , and associated velocity perturbations. An additional small-scale component was also included, ranging from  $\lambda_{\min} = 0.1$  to  $\lambda_{\max} = 0.5$ . The ratio of the small-scale component was taken as one-half that of the large-scale component at the coherence length,  $\lambda_w = 0.5$ . A power-spectrum index  $n = 0$  was assumed for each component.

Four random realizations of each of the different cosmological scenarios were performed. The same random number sequences were used in selecting the wavenumbers and phases for the different scenarios, so as to allow intrinsic differences to be separated from stochastic occurrences.

Naturally, great care must be taken to ensure that the procedures outlined above do indeed adequately represent the desired initial power spectrum within the range of interest for clusters. This procedure was checked by a variety of means, all of which confirmed that the desired initial fluctuation spectrum was indeed faithfully reproduced (Paper I; see also Braun and Dekel 1987).

c) *Large-Scale Cosmological Simulations*

Large-scale cosmological simulations were performed with  $\sim 4000$  equal-mass particles using a comoving direct  $N$ -body code (Aarseth 1984). This code integrates directly the Newtonian equations of motion in three dimensions using a softened gravitational potential,

$$\Phi = -Gm_i m_j / (r_{ij}^2 + \varepsilon^2)^{1/2} \quad (5)$$

where  $m_i$  and  $m_j$  are the masses of two particles,  $r_{ij}$  is their separation, and  $\varepsilon$  is the softening length. In these large-scale simulations, the comoving value of  $\varepsilon$  varies inversely with the expansion factor,  $a(t)$ , with an initial value  $\varepsilon = 0.03$  at the start of the simulation. The direct-summation  $N$ -body method was best suited for the present study, since accurate resolution of forces on small-scale is required if one desires high-resolution simulations of clusters and small-scale structure.

The stages of the simulations that correspond to the present epoch were determined by comparing the slope of the two-point correlation function,  $\xi(r)$ , in the low nonlinear regime with the slope of the observed galaxy correlation function. Equating the correlation length,  $r_0 = 0.1$  of the simulations to the claimed value for galaxies,  $r_0 \approx 5 h^{-1}$  Mpc (Davis and Peebles 1983; although see Oemler *et al.* 1987), then sets the scaling from model to physical units. Next rich clusters were identified in these large-scale simulations using the "friends-of-friends" procedure described in Paper I. For a given value of separation parameter,  $d$ , all particles closer to one another than this distance were linked together. Particles that are linked to each other, either directly or indirectly, form a cluster. The parameter  $d$  is related to the number overdensity,  $n/\langle n \rangle$ , at the outer edges of the cluster, via  $n/\langle n \rangle = (d/d_0)^{-3}$ , where  $d_0$  is the mean separation between neighbors in a Poisson distribution for the same number density of particles,  $d_0 = (V/N)^{-1/3}$ , and  $N$  is the total number of particles contained within the simulation volume  $V$ . The value of  $d$  used here to identify the rich clusters in these large-scale simulations corresponds to an overdensity of  $\sim 35$  at the edges of the clusters. Clusters identified using this procedure were found to contain typically 30–50 particles, each of mass  $m = 3.7 \times 10^{13} M_0$ . However, as previously discussed, because the aim here is to study the detailed

structure of these clusters and their surrounding region, such few particles of such large mass cannot provide sufficient resolution on small scales. It is for this reason that the second, high-resolution step was taken to create the final cluster models used in later analysis.

d) *Simulations of Individual Clusters*

Having identified the locations where rich clusters formed for a given set of initial perturbations, new simulations were performed using these same initial conditions but now modeling with higher resolution smaller volumes centered on the locations of each of the five richest clusters found in each of the large-scale simulations. In this way the resolution can be greatly increased, since by concentrating on the relatively small volume around each cluster, the mass of each individual particle in the new simulations can be much smaller, and more of the particles in the simulated volume eventually end up in the cluster itself rather than in other surrounding structures. The initial radius of these individual cluster simulations corresponds to 45% of the initial radius of the large-scale simulations. This volume size was chosen since it is sufficiently small to achieve the desired high resolution, yet sufficiently large that it still includes the relevant surrounding structures. As a check, several simulations were run with larger volumes, and it was found that no significant differences resulted in the structure of the clusters (see Paper I). High-resolution simulations with  $\sim 1000$  particles were run for each cluster using a non-comoving version of the Aarseth code, with each particle in these new simulations corresponding to roughly an  $L^*$  galaxy (Paper I). A fixed softening length  $\varepsilon = 0.01$  in models units was used, which should be comparable to the size of a typical galaxy,  $\varepsilon \approx 50$  kpc with the scaling of the previous section. Twenty clusters were simulated for each of the cosmogonic scenarios considered here, a total of 120 clusters. Figure 1 shows several representative clusters formed in each of the different scenarios. The effects of the different initial fluctuation spectra are illustrated even more clearly in Figure 2, where in each column is shown a different cluster that formed in the same location in each of the different large-scale simulations which used the same random number sequence to generate the initial conditions. Thus, the apparent differences in the visual appearance of the cluster formed in the different scenarios reflect the differences in the small-scale component of the initial perturbation spectrum.

The next objective was to quantify in a statistically meaningful way the amount of substructure within these clusters. Because the ultimate goal is to compare the simulated clusters with observed ones, it is important to treat the simulated clusters in much the same way that an observer would. Three orthogonal, projected views of each of the simulated clusters were used, at those times corresponding to the present epoch. A cubic volume with origin at the center of the simulated volume was cut to ensure equal depth along the line of sight. The cluster's center in each case was taken as the location of the density maximum of the projected distribution of particles within this cube, as determined by an iterative count procedure in square grid cells. This procedure was found to work quite well; in all cases, the cluster center determined by this procedure agreed well with that determined from visual inspection of the particle distribution. The cluster radius,  $R_{100}$ , was then determined by finding the radius at which the projected cluster density profile first falls to the mean background density, and the total cluster mass then found by counting all particles

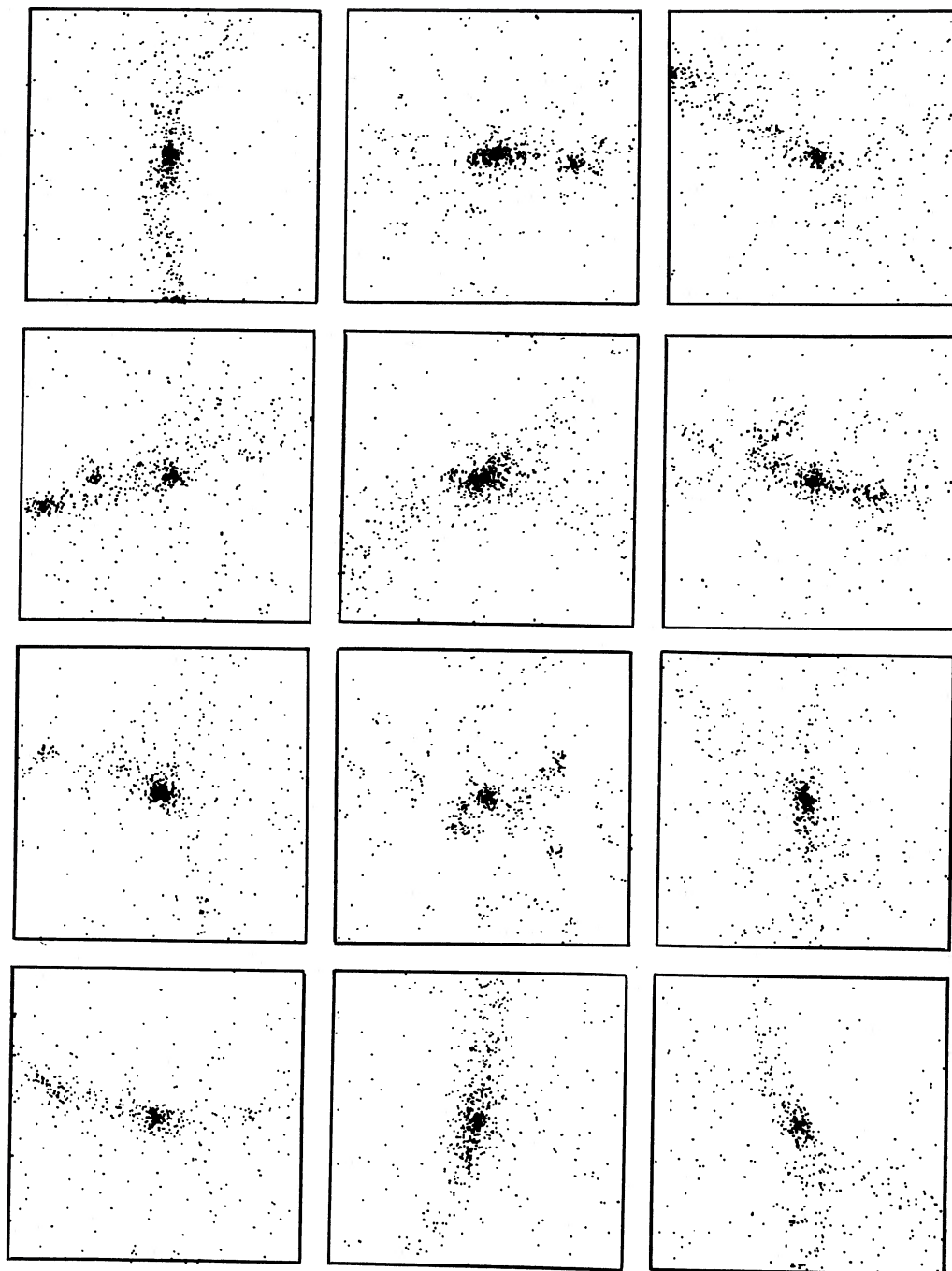


FIG. 1a

FIG. 1.—Typical clusters formed in the different cosmogonic scenarios, at those stages corresponding to the present epoch. The length of each box is  $20 h^{-1}$  Mpc. (a) Pancake; (b) hybrid; (c) hierarchical ( $n = 0$ ); (d) hierarchical ( $n = -1$ ); (e) hierarchical ( $n = -2$ ); (f) hierarchical ( $n = 0, \Omega = 0.15$ ).

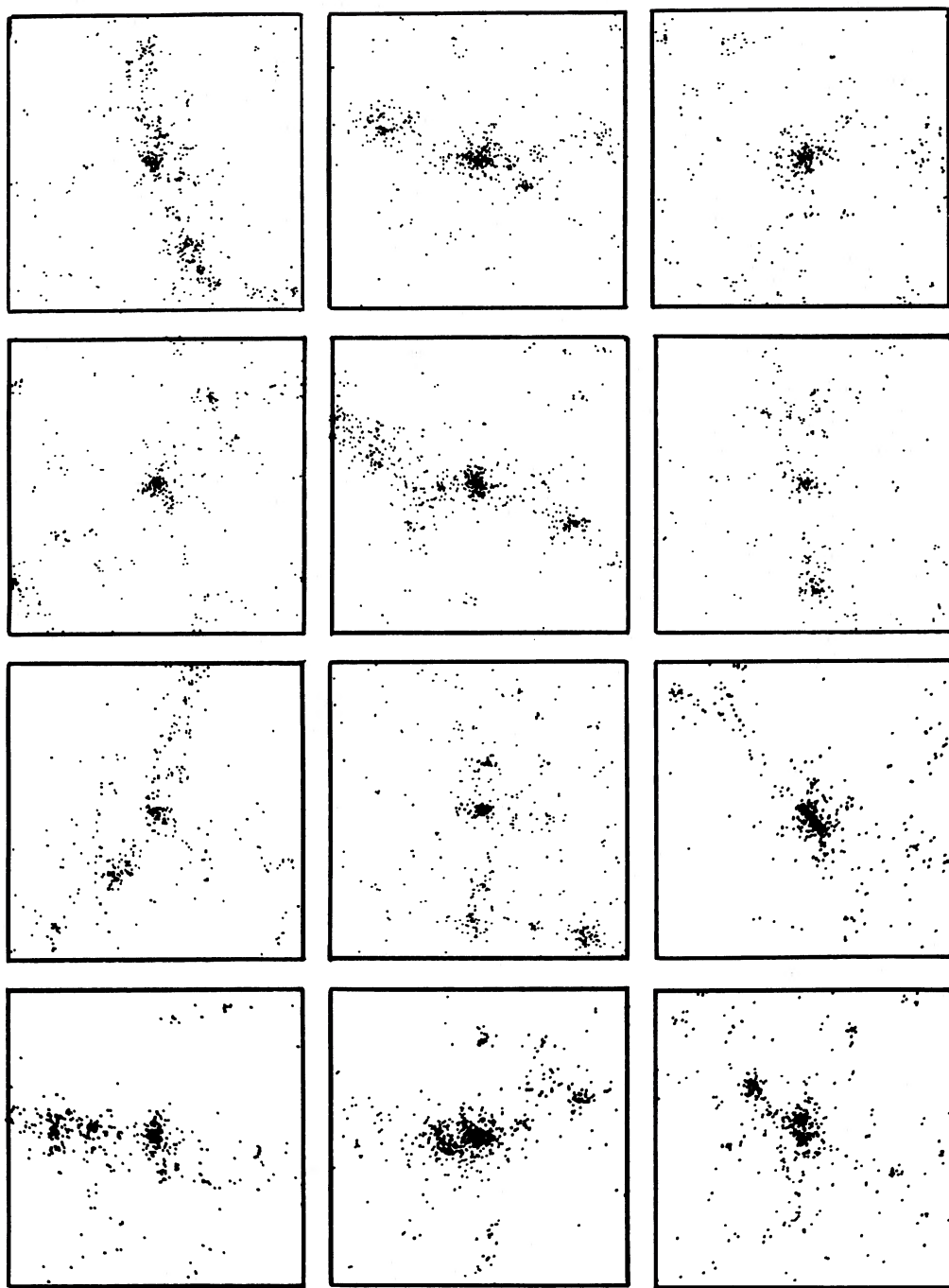


FIG. 1b

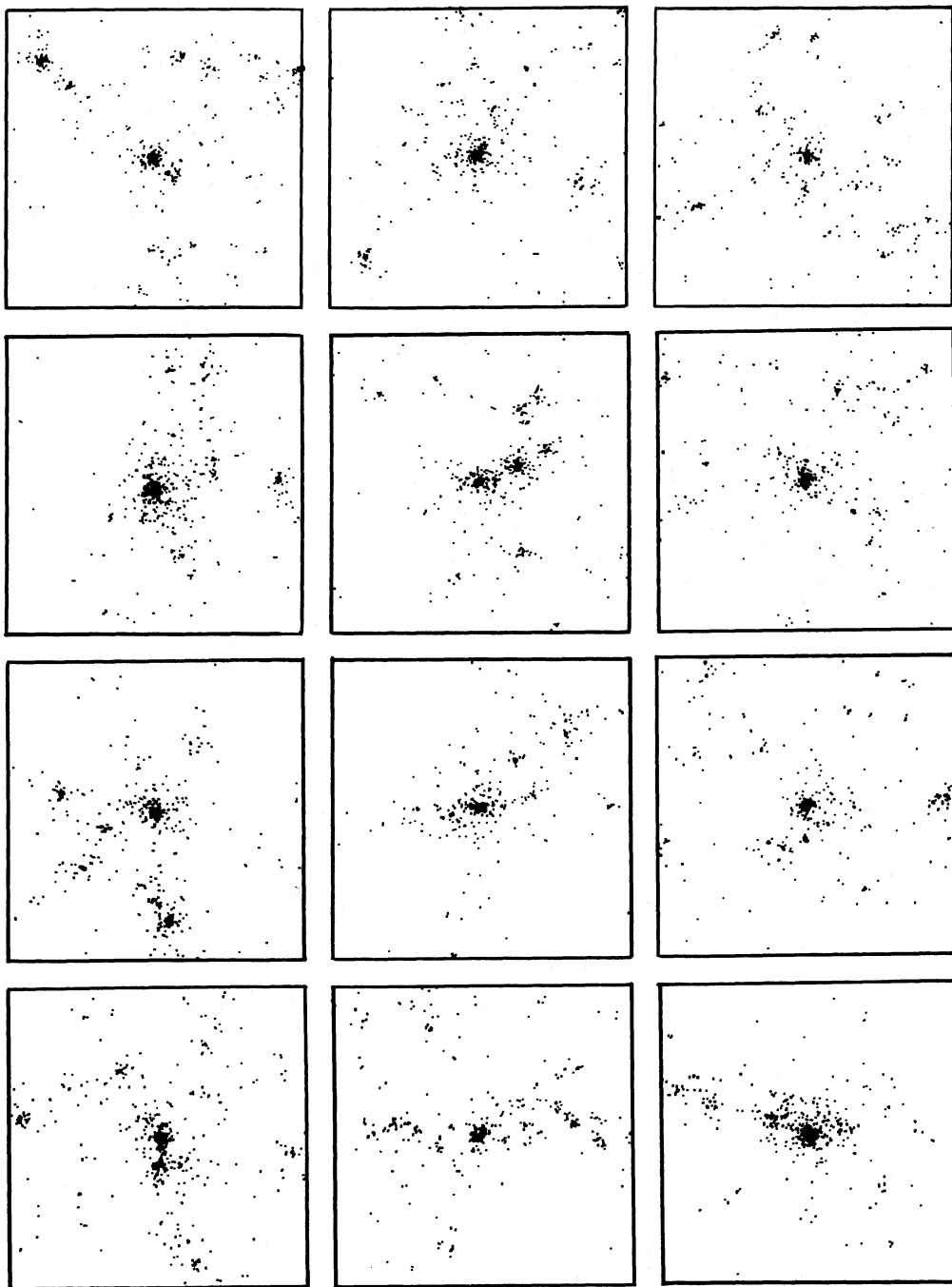


FIG. 1c

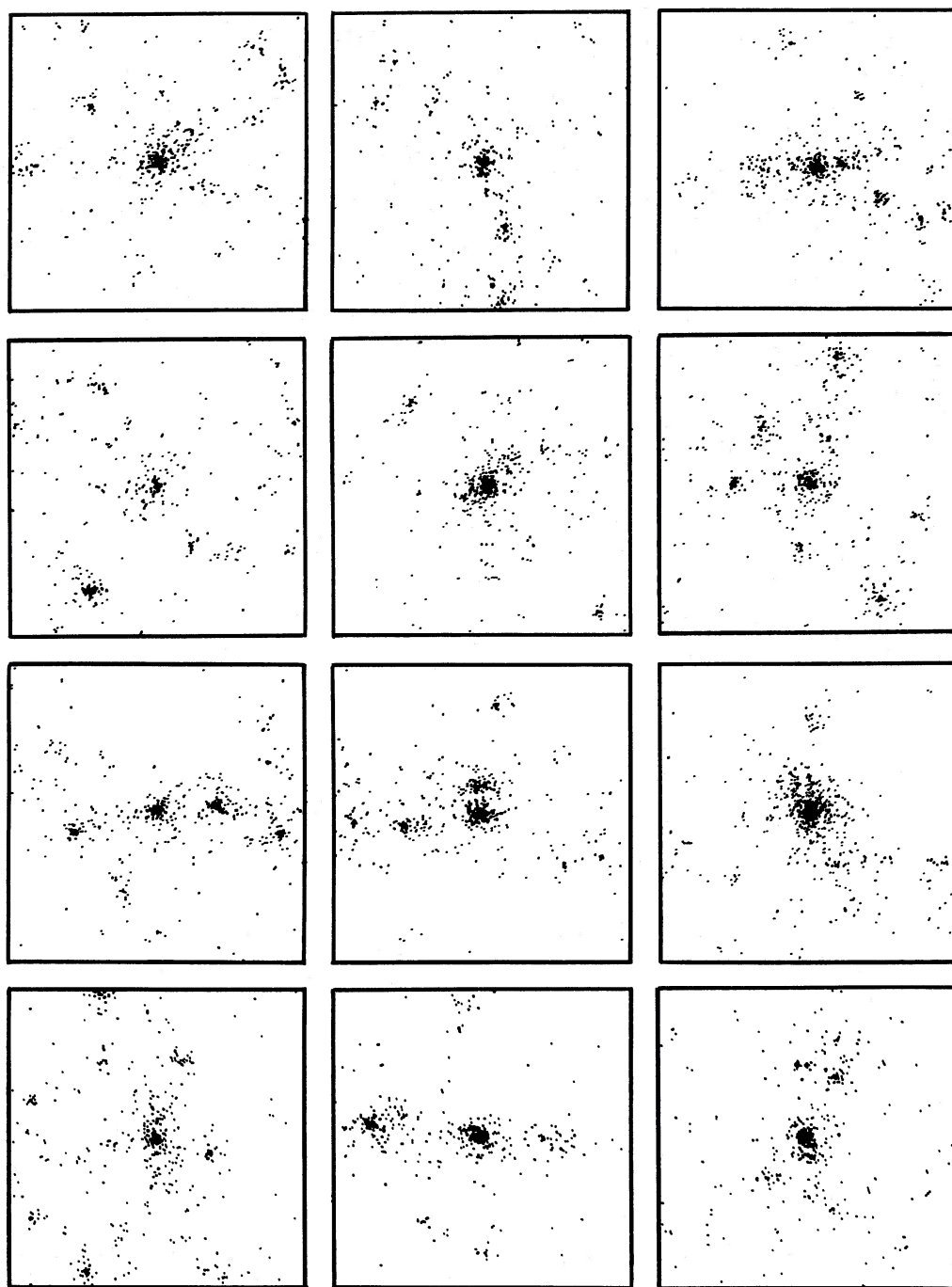


FIG. 1d

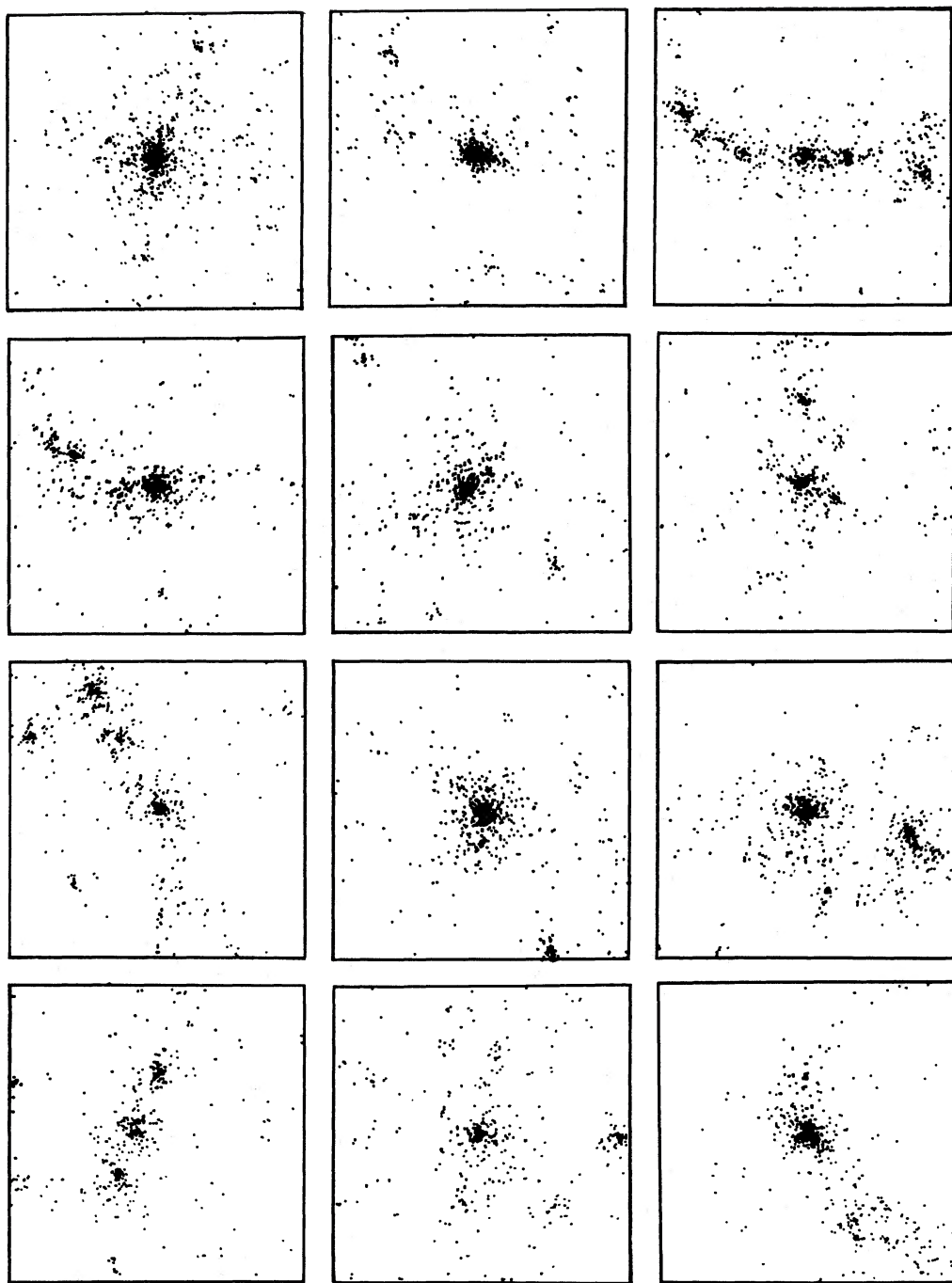


FIG. 1e

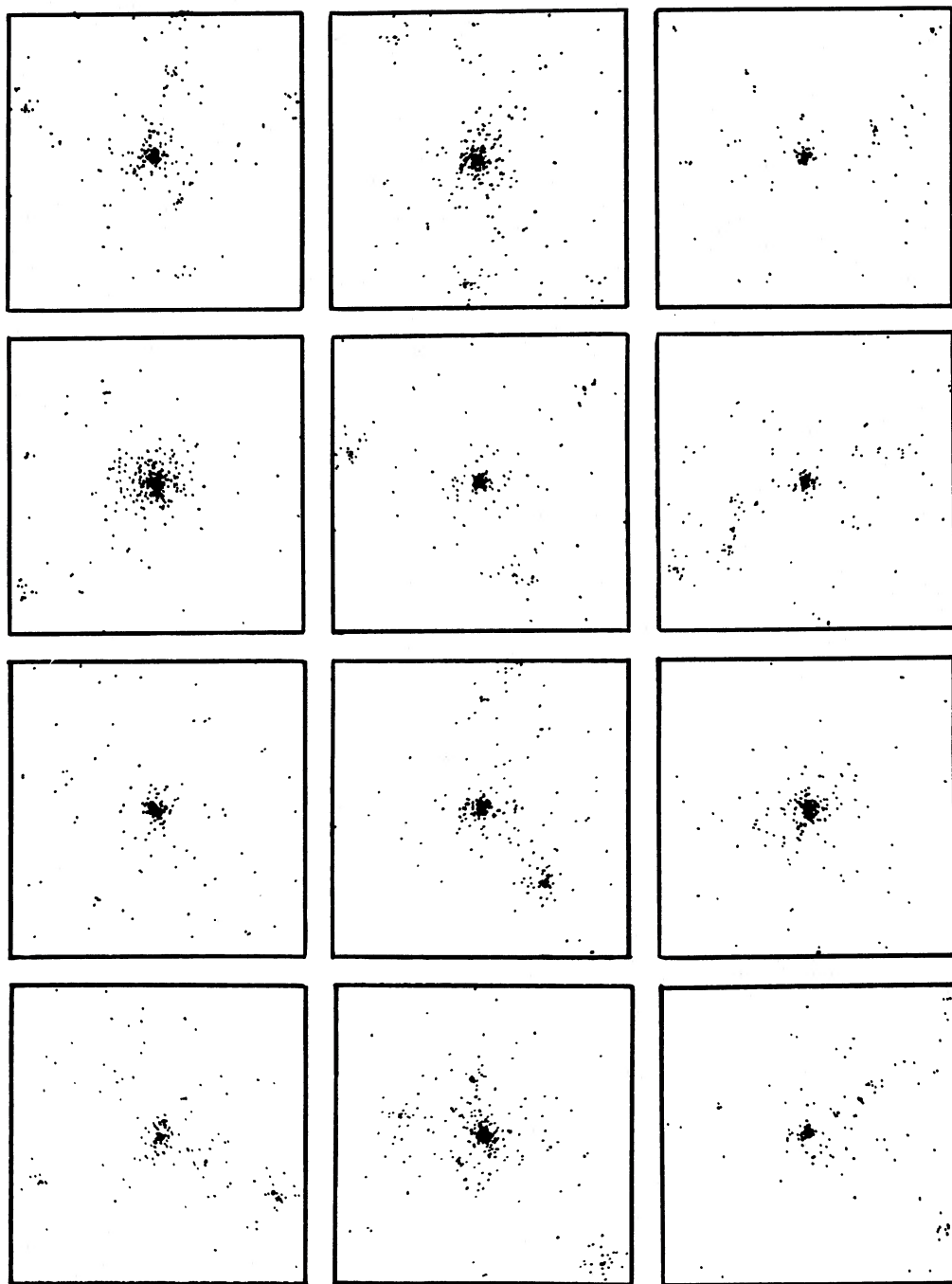


FIG. 1f

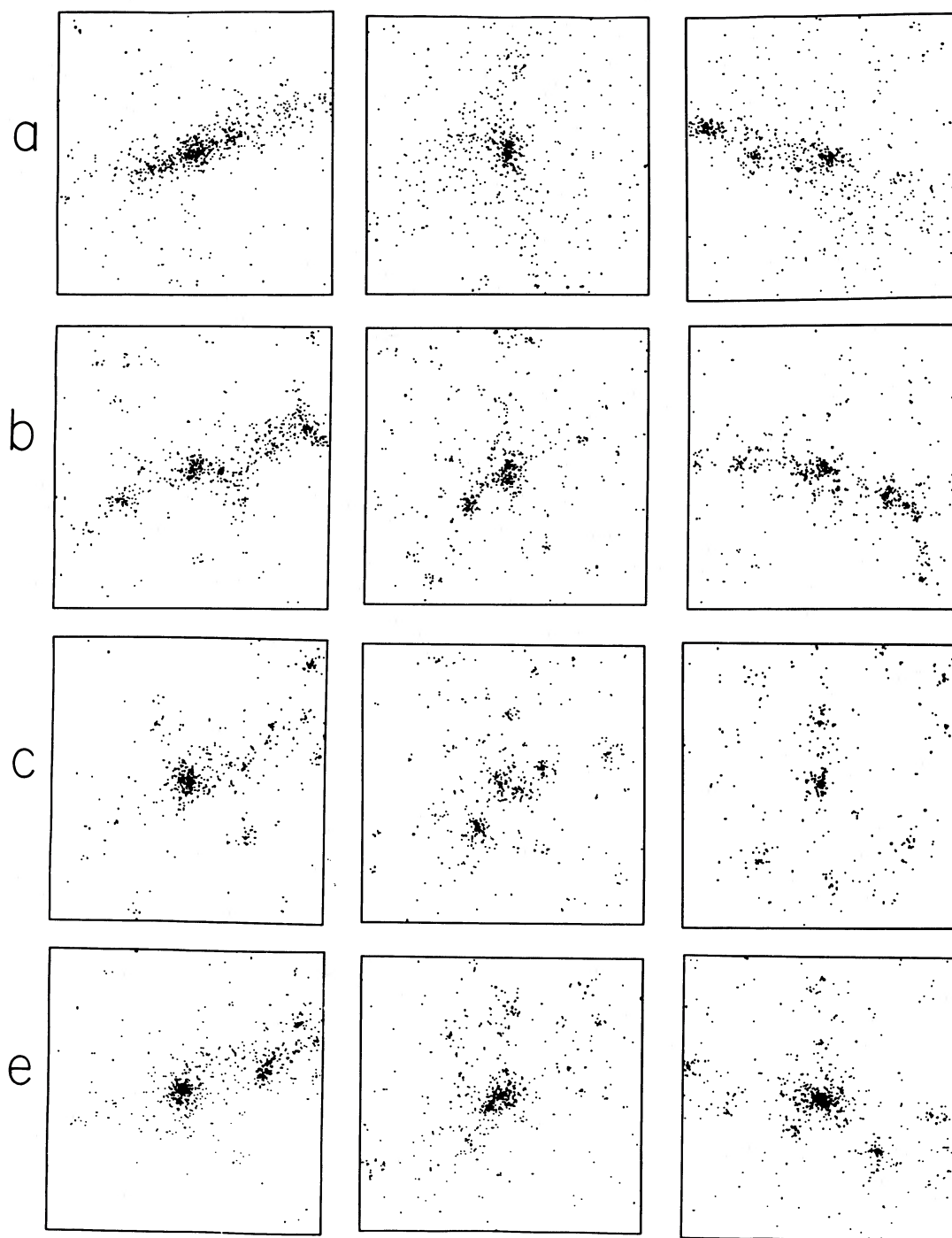


FIG. 2.—Illustration of the effects of different initial fluctuation spectra on the structure of rich clusters. Labels correspond to the scenarios listed in Table 1. Row a shows three typical clusters formed in simulations of the pancake scenario. Row b shows these same three clusters as they formed in the hybrid simulations. Rows c and e are these same three clusters as they formed in the  $n = 0$  and  $n = -2$  hierarchical clustering scenarios. Thus, the apparent differences in the clusters formed in the pancake, hybrid, and  $n = 0$  hierarchical clustering scenarios reflect differences in the amount of small-scale power present in the initial fluctuation spectrum, while differences in the  $n = 0$  and  $n = -2$  hierarchical clustering cases demonstrate the effects of having more power on large scales.

within this radius (see Paper I). The cluster half-mass radius,  $R_{50}$ , was taken as the radius encompassing half this total mass. Given the scaling of § IIc the typical half-mass radii of these clusters range roughly from 0.5 to  $1 h^{-1}$  Mpc, depending somewhat on the cosmological scenario. For example, the mean value of the half-mass radius is  $\langle R_{50} \rangle = 0.84 \pm 0.15 h^{-1}$  Mpc for clusters formed in the pancake simulation, while  $\langle R_{50} \rangle = 0.48 \pm 0.15 h^{-1}$  Mpc for those formed in the  $n = 0$ ,  $\Omega = 1$  hierarchical clustering scenario. Similarly,  $\langle R_{100} \rangle = 3.31 \pm 1.08 h^{-1}$  Mpc for the pancake clusters, and  $\langle R_{100} \rangle = 2.49 \pm 0.75 h^{-1}$  Mpc in the hierarchical clustering case. However, because of the uncertainties in the correlation functions used to set the scaling from model to physical units, these differences should not be taken as very significant.

### III. TESTS FOR SUBCLUSTERING

To provide a quantitative description of the presence and significance of substructure within clusters, three new statistical tests have been developed. These have been designed to eliminate possible contributions from global deviations from homogeneity, such as the overall falloff of the cluster density with radius, and global deviations from spherical symmetry, such as flattening of the mass distribution.

#### a) Description of Statistical Tests

##### i) Symmetry Test

This test quantifies the overall mirror symmetry of the galaxy distribution within a cluster about its center, on the premise that a subcluster represents a localized asymmetry superposed on an otherwise symmetric distribution. For each particle (or galaxy),  $i$ , the local density around that particle is estimated by finding the mean distance to its five nearest neighbors in projection,  $d_i$ . Then the local density in the vicinity of a point  $o$ , which is diametrically opposite the cluster center from particle  $i$ , is measured by the mean distance to the five nearest neighbors around this point,  $d_o$ . If the particle distribution is indeed symmetric, on average  $d_i$  and  $d_o$  should be roughly equal, while if the particle distribution is clumpy, then  $d_i$  and  $d_o$  should in general be different. As a measure of any asymmetry, a statistic  $\beta$  was defined by

$$\beta = \log_{10}(d_o/d_i), \quad (6)$$

and the average value of  $\beta$  over all particles provides a measure of any gross deviations from symmetry. For a symmetric distribution  $\langle \beta \rangle \approx 0$ , while values of  $\langle \beta \rangle$  greater than 0 indicate the presence, and significance, of any asymmetries. Since this is done about each particle,  $\langle \beta \rangle$  is a density-weighted average, and thus is more sensitive to the presence of substructure than if random points were selected within the cluster. The value of  $\beta$  also depends on the density of the clumps themselves, with more compact lumps producing a larger value. It is also possible to examine the trend of symmetry/asymmetry with distance from the cluster center,  $\beta(r)$ , to look for any systematic trends of subclustering with radial distance. In practice, global values of  $\beta$  were measured for two separate regions; for particles in the ranges  $0 < r < R_{50}$  and  $R_{50} < r < R_{100}$ .

One of the primary advantages of this test is that it is unaffected by any global flattening of the particle distribution, which could generate a false signal of subclustering with some tests which assume spherical symmetry of the galaxy distribution. In addition, even in the absence of any "significant" localized subclustering, this test can provide a measure of the overall regularity or irregularity of the mass distribution,

which might provide a crude means for determining the approximate dynamical state of a given cluster.

##### ii) Angular Separations Test

If one considers the distribution of galaxies within a cluster in terms of only angular coordinates about the cluster center (relative to some arbitrarily defined fixed coordinate axis), the presence of any subclustering will clearly result in an excess number of small angular separations between galaxy pairs relative to the corresponding number expected in a spherically symmetric, subcluster-free distribution. Thus, examining the distribution of angular separations between pairs of cluster galaxies may provide a simple and useful test for substructure. Because it is the distribution of small angular separations that is of most interest here, it is more useful to calculate the harmonic mean value of the angular separations rather than, say, the mean or median value, since the harmonic mean is weighted most by small values. The harmonic mean angular separation is defined by

$$\theta_{\text{hm}} = \left[ 2/N(N-1) \sum_{i>j} \theta_{ij}^{-1} \right]^{-1}, \quad (7)$$

where  $\theta_{ij}$  is the angular separation between particles  $i$  and  $j$ , and the sum is over all pairs,  $N$  being the total number of particles. The useful measure is the ratio of  $\theta_{\text{hm}}$  measured for the cluster over that for a Poisson distribution of the same number of particles,  $\theta_{\text{hm}}/\theta_p$ . This ratio should be  $\sim 1$  if no subclustering is present, while it will be less than 1 if there is substructure. In application, the harmonic mean angular separation of the particle distribution was computed using the same two radial bins used for the symmetry test,  $0 < r < R_{50}$ , and  $R_{50} < r < R_{100}$ . The corresponding harmonic mean values expected for a random distribution of  $N$  particles were computed by averaging over 1000 Monte Carlo simulations which were generated for selected values of  $N$  in the range  $20 < N < 500$ , and by interpolation between these values. These were generated by selecting  $N$  angles,  $\theta$ , uniformly at random in the range  $0-2\pi$ , and computing the harmonic mean angular separation for the given distribution. After some testing, it was found that the stability of this statistic could be significantly improved by imposing a lower limit to the angular separations considered, since even in a Poisson distribution the occasional rare pair of exceedingly small separation can give rise to rather wild fluctuations in the harmonic mean values. By rejecting all pair separations less than 1% of the expected mean interparticle separation if the  $N$  particles were uniformly distributed (i.e.,  $0.01[2\pi/N]$ ), this statistical test becomes much more robust. This is not at all a harsh constraint imposed on the allowable separations: for example, in a Poisson distribution of  $N = 500$  particles ( $N_{\text{pairs}} \approx 500^2/2$ ) the average number of pairs rejected in each of the 1000 Monte Carlo simulations was only  $\sim 5$ .

This angular separations test provides a nice complement to the aforementioned symmetry test, since it yields information about the spectrum of interparticle angular separations, which will be affected by the presence of say, a single, large subcluster, or by a galaxy distribution dominated by an excess of small groups, binaries, or both (e.g., Struble and Rood 1981). Also, when applied to a given radius interval, this test is insensitive to the radial mass distribution within the clusters. (In principle, one might use the harmonic mean value of the projected spatial separations between pairs as a measure of subclustering; Quintana, de Souza, and Arakaki 1986. However, such a test is probably too sensitive to the shape of the cluster

density profile to provide unambiguous evidence for the presence of subclustering.) The principal disadvantage of this method is that the two-dimensional projected galaxy distribution is reduced to a single angular dimension, with a corresponding loss of some information. Also the angle subtended by substructure of a given physical size will obviously depend on its distance from the cluster center, so a meaningful analysis must be confined to a limited radius interval. Finally, unlike the symmetry test, flattening of the particle distribution might affect  $\theta_{\text{hm}}$ , by biasing the angular separations toward small values even in the absence of genuine subclustering. As it turns out, though, cluster ellipticity does not seem to have a great effect on this statistic (see § IIIb).

### iii) Density Contrast Test

An interesting property of any detected substructure is the fraction of the total cluster mass which is actually contained in the clump or clumps, as well as the distribution of subcluster masses. For example, a single "subcluster" composed of, say, five galaxies in a cluster of 200, while perhaps representing a true physical association, is hardly of consequence for the dynamics of the cluster as a whole, since even in relaxed clusters outlying groups will continue to fall in at later times (e.g., Gunn and Gott 1972). Also because the three-dimensional galaxy distribution in clusters is viewed in only two dimensions, some apparent subclusters and lumps may in fact be nothing more than projection effects or random fluctuations. Obviously, then, the existence and significance of substructure are very subjective.

In an attempt to quantify the significance of subclustering, a test was used which employs a group-finding algorithm to locate all separate clumps of a specified density contrast in each cluster using the "friends-of-friends" method described in § II. One can then examine the number and sizes of these clumps at different density contrast levels in order to search for the existence of distinct subclusters which contain a significant fraction of the total cluster mass or binding energy, or both. For each cluster of galaxies, all separate groups within the cluster were identified for density contrast levels of  $\rho/\langle\rho\rangle = 5, 10, 20, 40, 60, 80, 100, 150, \text{ and } 200$ . At the lowest density levels, almost all cluster particles are joined together to form a single group, while at the very highest density contrasts only small dense groups and isolated pairs are identified. If significant subclustering is truly present, one would expect that as the density contrast level is raised, at some point the cluster distribution should "fragment" into several distinct and sizable lumps. The majority of the clusters showing substructure in the density contour plots of Geller and Beers (1982) seem to possess one or two subcondensations at various distances from the cluster center. Other  $N$ -body simulations of cluster formation via hierarchical clustering (e.g., White 1976; Cavaliere *et al.* 1986) have also shown that during the collapse phase subclustering often occurs in the form of several prominent clumps which subsequently merge to form a single, relaxed cluster. Thus, as a measure of the "significance" of subclustering, the maximum fractional mass contained in the second and third largest subclusters found at any of the different density contrast levels,  $S_{2\text{max}}$  and  $S_{3\text{max}}$ , was examined (the largest "subcluster" is always due just to the fact that the cluster mass distribution is centrally concentrated). This density contrast test somewhat resembles the method used by Geller and Beers, although the test used here studies the mass fraction contained within a subcluster in addition to its density

enhancement. This test does not assume any specific shape of the subclusters.

It is worth reiterating that these three tests for subclustering are not simply redundant ways of measuring the same property. Each is sensitive to a different aspect of subclustering, and thus they are complementary measures.

### b) Checks of Subclustering Tests

It is important to calibrate the results of these statistical tests, and to make sure that they do indeed succeed in detecting any significant substructure which may be present in the clusters, without generating spurious signals. These methods were first tested on a set of "artificial" clusters which were generated by a Monte Carlo technique. In principle, one could have generated such clusters by assuming a specific shape for the density profile (say an  $r^{1/4}$  profile, or Hubble profile), and then distributing  $N$  particles according to this prescription. However, although the results of the symmetry and angular separations tests are independent of the cluster radial mass distribution, there is a chance that the choice of density profile might affect in subtle ways the detection of lumps of a given size using the density contrast test. Instead, to guarantee that the radial mass distribution of these artificial clusters was identical to that of the simulated clusters without needing to choose some analytic form for the cluster profile, the simulated clusters themselves were used to create the artificial clusters. For the particle distribution within a given simulated cluster, a corresponding artificial cluster, with no substructure, was generated by keeping the radial coordinate of each particle the same, but assigning randomly chosen angular coordinates. In this way, artificial clusters were created which have three-dimensional radial mass distributions identical to those of the simulated clusters, but possess no subclustering, due to the randomly chosen angular positions. Twenty such artificial clusters were generated in this manner, each being based on a different simulated cluster. One such artificial cluster is shown in Figure 3a. The tests for subclustering were then applied to three orthogonal projected views of each of these clusters. For this sample, the mean value of the symmetry index was found to be

$$\langle\beta\rangle = 0.003 \pm 0.036 \quad \text{for } 0 < r < R_{50},$$

$$\langle\beta\rangle = 0.001 \pm 0.039 \quad \text{for } R_{50} < r < R_{100},$$

while the mean values found for the angular separations test were

$$\langle\theta_{\text{hm}}/\theta_{\text{p}}\rangle = 0.986 \pm 0.109 \quad \text{for } 0 < r < R_{50},$$

$$\langle\theta_{\text{hm}}/\theta_{\text{p}}\rangle = 1.007 \pm 0.106 \quad \text{for } R_{50} < r < R_{100}.$$

Hence, these two tests behaved as expected, demonstrating the lack of any significant subclustering. The distribution of values of  $S_{2\text{max}}$  found for these artificial clusters using the density contrast test is shown in Figure 4. The mean values of  $S_{2\text{max}}$  were  $\langle S_{2\text{max}}\rangle = 0.050 \pm 0.021$  and  $\langle S_{3\text{max}}\rangle = 0.032 \pm 0.015$ . Thus it seems that even in a galaxy distribution which is free of any genuine subclustering, clumps containing 5%–10% of the total cluster mass are expected to occur simply from random fluctuations and projection effects. Indeed, nearly one-third of these "subcluster-free" artificial clusters were found to possess clumps containing 5%–15% of the total mass. Furthermore, if the cluster is flattened, one could expect to find even larger values of  $\langle S_{2\text{max}}\rangle$  and  $\langle S_{3\text{max}}\rangle$  even in the absence of any genuine subclustering.

As mentioned earlier, there is some danger that flattening of the galaxy distribution might generate a false signal of subclustering with the angular separations test. To check just how serious this effect is, a sample of artificial clusters was generated whose distribution of observed ellipticities matched that of the clusters formed in the pancake simulations (Paper III), with ellipticities in the range  $0.0 < \varepsilon < 0.5$ . The resulting distribution of values of  $\langle \theta_{\text{hm}}/\theta_{\text{p}} \rangle$  for these artificial clusters was found to be fairly insensitive to such elongations, with a mean value  $\langle \theta_{\text{hm}}/\theta_{\text{p}} \rangle = 0.09 \pm 0.15$  found for this sample. Further testing showed that this statistic is reasonably unaffected by

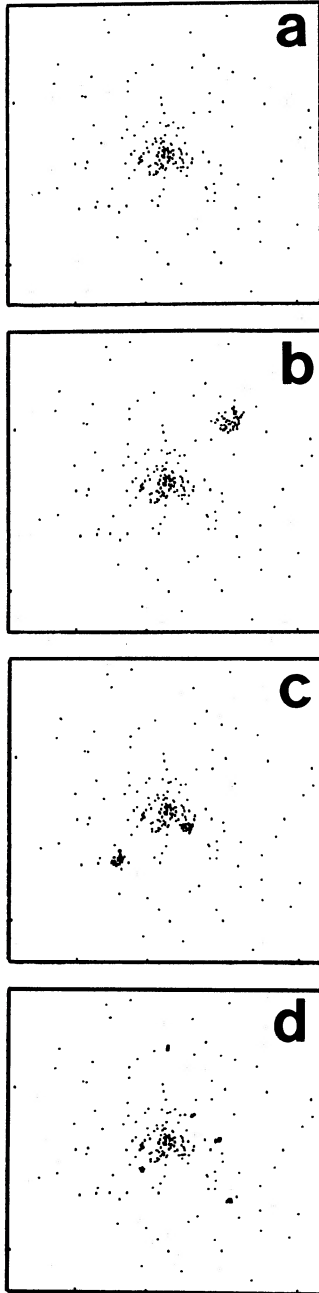


FIG. 3.—An artificial cluster, generated by the technique described in the text. (a) Cluster without any subclustering; (b), (c), and (d) same cluster with subclustering superposed, as described in the text. The length of each box corresponds to  $5 h^{-1}$  Mpc.

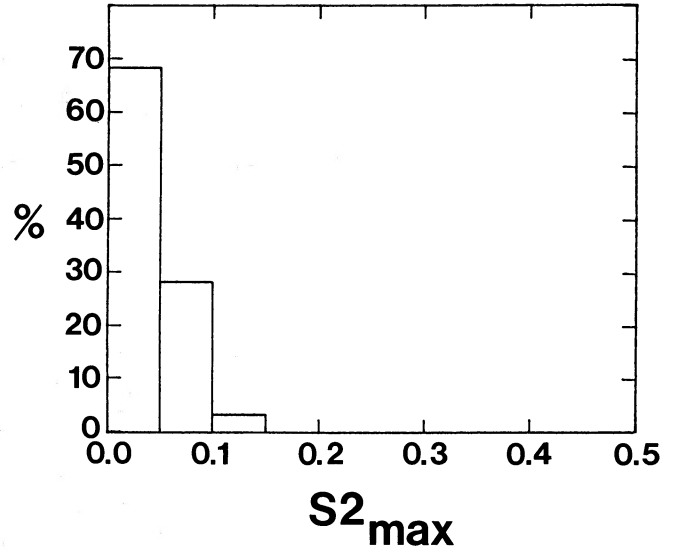


FIG. 4.—Distribution of values of  $S2_{\text{max}}$  for the set of artificial (subcluster-free) clusters.

flattening for ellipticities up to  $\varepsilon \sim 0.5$  although larger values of  $\varepsilon$  were found to strongly bias  $\theta_{\text{hm}}$  to small values, thus producing a false signal of subclustering. However, within the range of ellipticities appropriate for the clusters studied here, the angular separations test is fairly unaffected by flattening of the cluster mass distribution.

Having demonstrated that these tests do not produce spurious signals of subclustering, the next step is to show that they are indeed sensitive to any significant substructure which may be present. To do this, different types of subclustering have been superposed on the field of the artificial cluster shown in Figure 3a, and the statistical tests then rerun. Figure 3b shows the addition of a single, large subcluster. This subcluster is located beyond the cluster half-mass radius and contains  $\sim 20\%$  of the total cluster mass, distributed randomly within a sphere of radius  $0.25 h^{-1}$  Mpc. In Figure 3c two smaller subclusters were added to the original cluster, one located interior to  $R_{50}$ , the other beyond  $R_{50}$ . Each contains 10% of the total mass, distributed randomly within spheres of radii 0.10 and  $0.15 h^{-1}$  Mpc. And in Figure 3d, five very small, dense knots have been superposed on the cluster, each containing  $\sim 5\%$  of the cluster mass, distributed within spheres of radius  $0.05 h^{-1}$  Mpc. Application of the three statistical tests yielded the results shown in Table 2. Note that all three tests for subclustering detect the presence of these different kinds of substructure, although for a given type of subclustering one test may be more sensitive than the others. If numerous subclusters had been included, or if these subclusters contained an even greater fraction of the total cluster mass, or if the particles within the subclusters were themselves clustered rather than randomly distributed, then these tests would give an even stronger signal of substructure. However, these simple cases serve to demonstrate that these tests are indeed capable of detecting substructure when present.

#### c) Application of Tests to Simulated Clusters

These three statistical tests for subclustering were then applied to the entire set of simulated clusters, using projected views. The results for each of the different scenarios are shown

TABLE 2  
CHECKS OF SUBCLUSTERING TESTS

CLUSTER	$\beta$		$\theta_{\text{hm}}/\theta_{\text{p}}$		$S2_{\text{max}}$
	$0 < r < R_{50}$	$R_{50} < r < R_{100}$	$0 < r < R_{50}$	$R_{50} < r < R_{100}$	
a.....	0.04	-0.01	1.02	1.09	0.04
b.....	0.03	0.20	0.99	0.41	0.21
c.....	0.37	0.22	0.59	0.74	0.12
d.....	0.13	0.24	0.68	0.61	0.05

in Figures 5–8. Mean values of these statistical measures are listed in Tables 3, 4, and 5. The results are briefly summarized below.

i) Results from Symmetry Test

Figures 5 and 6 show the distributions of values of  $\beta$  found for the regions  $0 < r < R_{50}$  and  $R_{50} < r < R_{100}$ , respectively. Mean values of  $\beta$  for all the different scenarios are listed in Table 3. For the innermost region, the mean values of  $\beta$  for all scenarios are similar within the statistical uncertainties and are consistent with little or no subclustering. For the region  $R_{50} < r < R_{100}$ , some differences can be seen between the various scenarios, with the least amount of substructure detected in

clusters formed in the pancake scenario, and the strongest signal of subclustering for clusters in the  $n = 0$ ,  $\Omega = 1$ , hierarchical clustering scenario. However, the values of  $\beta$  are generally not very large (compare to Table 3), which suggests that the substructure being detected is not very sizable.

ii) Results from Angular Separations Test

Figures 7 and 8 show the distributions of  $\theta_{\text{hm}}/\theta_{\text{p}}$  found from the angular separations test, for the same radial bins as above. Mean values are listed in Table 4. For the region  $0 < r < R_{50}$ , the mean values of  $\theta_{\text{hm}}/\theta_{\text{p}}$  for all scenarios are found to lie within one standard deviation of each other and are consistent with little significant subclustering in this region. For the

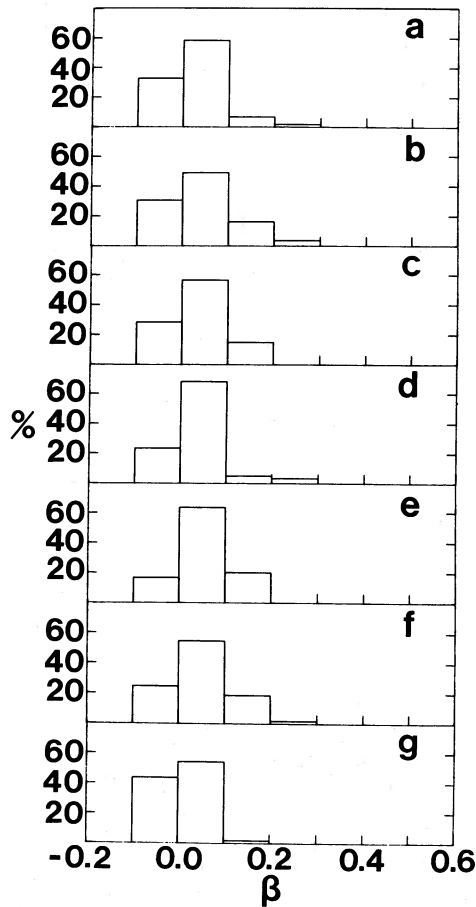


FIG. 5

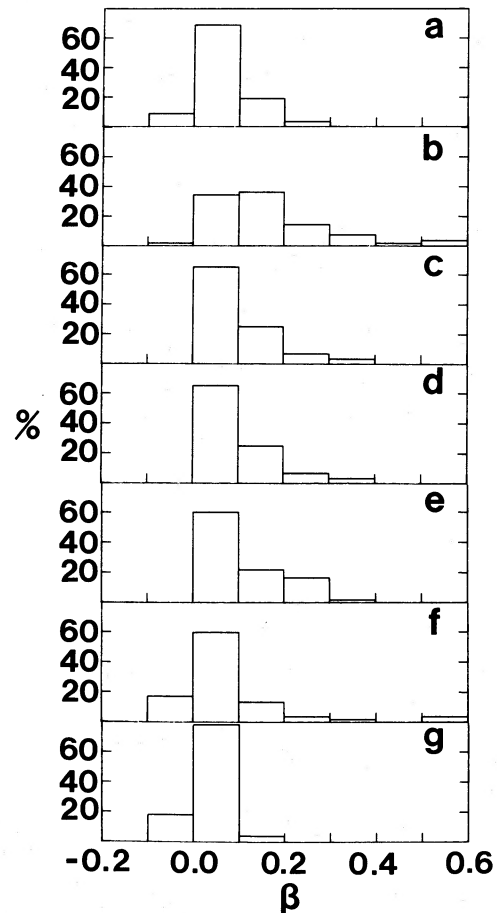


FIG. 6

FIG. 5.—Results of the symmetry test. Shown are the distributions of  $\beta$  for the region  $0 < r < R_{50}$ . Labels denote the following scenarios: (a) pancake, (b) hybrid, (c), (d), (e) hierarchical clustering ( $\Omega = 1$ ) for  $n = 0, -1$ , and  $-2$ , respectively, and (f)  $n = 0$  hierarchical clustering for  $\Omega = 0.15$ . (g) Distribution found for Dressler's sample of rich clusters.

FIG. 6.—Results of the symmetry test for the region  $R_{50} < r < R_{100}$ . Labels are the same as in Fig. 5.

TABLE 3  
MEAN VALUES OF  $\beta$

SCENARIO	$\langle\beta\rangle$	
	$0 < r < R_{50}$	$R_{50} < r < R_{100}$
Pancake .....	$0.01 \pm 0.06$	$0.07 \pm 0.07$
Hybrid .....	$0.02 \pm 0.04$	$0.15 \pm 0.12$
Hierarchical ( $n = 0$ ) .....	$0.04 \pm 0.04$	$0.16 \pm 0.12$
Hierarchical ( $n = -1$ ) .....	$0.03 \pm 0.04$	$0.11 \pm 0.07$
Hierarchical ( $n = -2$ ) .....	$0.03 \pm 0.06$	$0.11 \pm 0.04$
Hierarchical ( $n = 0, \Omega = 0.15$ ) .....	$0.04 \pm 0.06$	$0.08 \pm 0.12$
Abell clusters .....	$0.01 \pm 0.04$	$0.03 \pm 0.10$

region  $R_{50} < r < R_{100}$ , the mean values of this statistic suggest the presence of some substructure in these simulated clusters, with the pancake simulations again showing the weakest signal of subclustering and the  $n = 0, \Omega = 1$  hierarchical sub-

clustering scenario showing the strongest evidence. However, the mean values of  $\theta_{\text{hm}}/\theta_p$  for this outer region also lie within one standard deviation of each other for all scenarios.

iii) Results from Density Contrast Test

The distributions of values of  $S2_{\text{max}}$  are shown in Figure 9, and these results are summarized in Table 5. It is apparent that some signal of substructure is being detected in all scenarios. However, there are relatively few subclusters containing a large fraction of the total cluster mass. If an arbitrary criterion for "significant" substructure is set at, say  $S2_{\text{max}} \geq 20\%$  of the total cluster mass (remembering that 5%–10% fluctuations occur naturally due to random variations and projection effects; see § IIIb), then only  $\sim 5\%$  of clusters in the pancake scenario and  $\sim 8\%$  in the  $n = 0, \Omega = 1$  hierarchical clustering scenario meet this criterion. For a less stringent requirement,  $S2_{\text{max}} \geq 15\%$  of the total cluster mass,  $\sim 12\%$  of the pancake clusters, and  $\sim 28\%$  of the  $n = 0, \Omega = 1$  hierarchical clusters

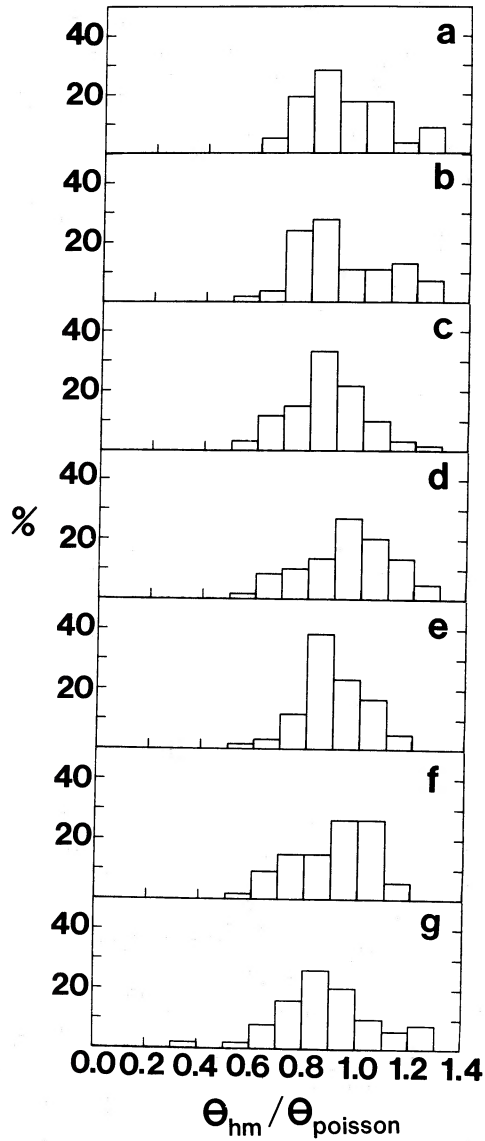


FIG. 7

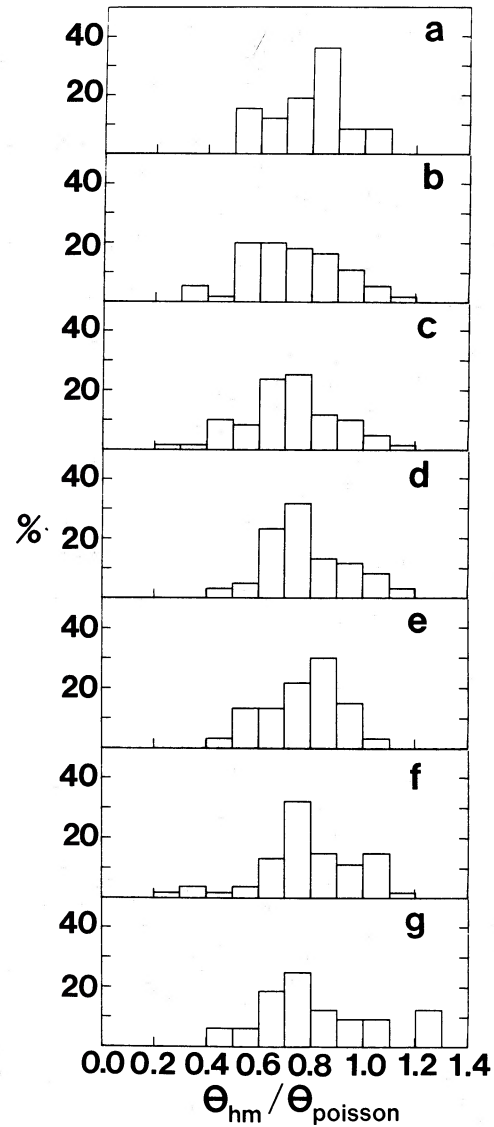


FIG. 8

FIG. 7.—Results of the angular separations test. Shown are the distributions of values of  $\theta_{\text{hm}}/\theta_p$  for the region  $0 < r < R_{50}$ . Labels are the same as in Fig. 5.  
FIG. 8.—Results of the angular separations test for the region  $R_{50} < r < R_{100}$ . Labels are the same as in Fig. 5.

meet this criterion. Thus, it is not uncommon to observe some subclustering at levels marginally above Poisson noise, although large subclusters are quite rare in these simulated clusters.

It is interesting to note that there is a general trend which goes in the sense one might have expected *a priori* on the basis of the small-scale component of the primordial power spectrum in each scenario. In the pancake scenario, little substructure is detected with these tests, a result which is not too surprising given the lack of small-scale fluctuations in the initial spectrum. The hierarchical clustering simulations, on the other hand, while exhibiting little evidence for significant substructure in the innermost regions, do show a signal for some subclustering at radii. Clusters formed in the hybrid scenario yield results essentially intermediate to those of the pancake and hierarchical clustering scenarios, which again is not too surprising. In general, though, the signal of substructure detected in these different scenarios is usually not very strong (compare to the cases in Table 2). The fact that only a small amount of significant subclustering is found in most of these simulated clusters, especially in their inner regions, suggests that they are most probably relaxed systems. Thus, it seems that subclustering within clusters cannot provide as useful a

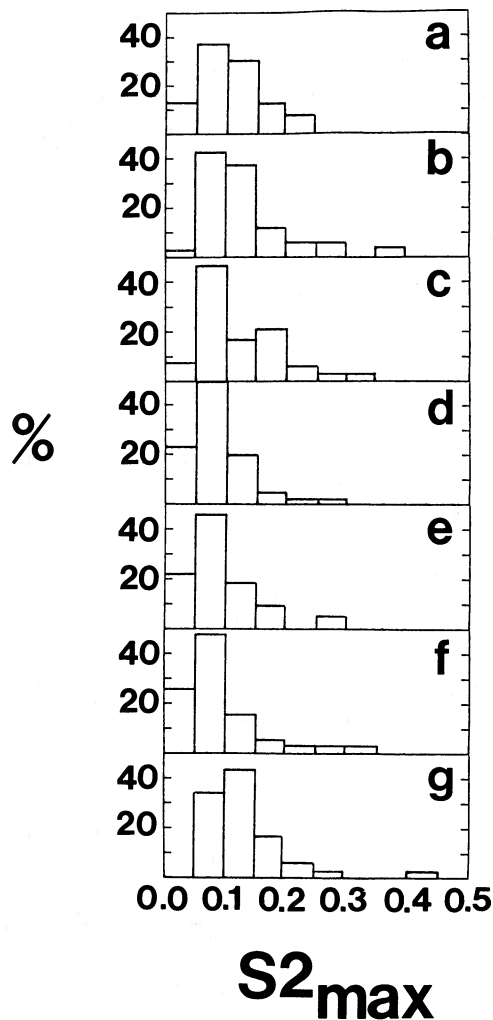


FIG. 9.—Distribution of values of  $S2_{\max}$  from the density contrast test. Labels are the same as in Fig. 5.

TABLE 4  
MEAN VALUES OF  $\theta_{\text{hm}}/\theta_{\text{p}}$

SCENARIO	$\langle \theta_{\text{hm}}/\theta_{\text{p}} \rangle$	
	$0 < r < R_{50}$	$R_{50} < r < R_{100}$
Pancake .....	$0.95 \pm 0.18$	$0.80 \pm 0.14$
Hybrid .....	$0.96 \pm 0.20$	$0.74 \pm 0.18$
Hierarchical ( $n = 0$ ) .....	$0.89 \pm 0.19$	$0.71 \pm 0.19$
Hierarchical ( $n = -1$ ) .....	$0.95 \pm 0.17$	$0.78 \pm 0.17$
Hierarchical ( $n = -2$ ) .....	$0.92 \pm 0.12$	$0.78 \pm 0.14$
Hierarchical ( $n = 0, \Omega = 0.15$ ) .....	$0.90 \pm 0.18$	$0.78 \pm 0.21$
Abell clusters .....	$0.90 \pm 0.18$	$0.82 \pm 0.22$

test of the different cosmogonic scenarios as had been originally hoped, since relaxation effects seem to have erased most traces of the initial conditions. Since the present epoch in these simulations was chosen on the basis of the correlation function of the large-scale galaxy distribution, this implies that most clusters should be expected to exhibit little significant substructure today. This is essentially consistent with the results of Cavaliere *et al.* (1986), who find that the number of “multicomponent” clusters should decrease rapidly at the present epoch, although they claim that only a small fraction of clusters should already be relaxed systems. However, as will be discussed shortly, there is some danger of selection effects when identifying clusters (in both the large-scale cosmological simulations and observationally as well) which may introduce significant biases here.

#### d) Subclustering in Observed Clusters

To compare the above results on subclustering in the simulated clusters with observed clusters, these same tests were applied to the sample of 55 clusters for which Dressler (1980b) has provided galaxy positions. Unfortunately, application of the symmetry and angular separations tests is complicated here by the fact that the measured area for each cluster is often quite small. These two tests can only be applied within an area defined by the largest circle, with origin at the cluster center, which can be drawn within the measured area. In some cases, this area is actually quite small, since the clusters are not always centered in the measured areas. The cluster centers were located using the same iterative procedure as was used for the simulated clusters (see § II; except A548, where the cluster center was taken as the center of the two distinct clumps because of the limited plate area). Crude measures of the cluster radius and half-mass radius were then obtained for each cluster by simply taking as  $R_{100}$  the distance of the fur-

TABLE 5  
RESULTS OF DENSITY CONTRAST TEST

Scenario	$\langle S2_{\max} \rangle$	$S2_{\max} > 0.20^a$	$S2_{\max} > 0.15^a$
Pancake .....	$10.9 \pm 5.1$	5%	17%
Hybrid .....	$11.7 \pm 5.4$	9%	20%
Hierarchical ( $n = 0$ ) .....	$12.6 \pm 5.8$	8%	28%
Hierarchical ( $n = -1$ ) .....	$9.0 \pm 4.5$	4%	18%
Hierarchical ( $n = -2$ ) .....	$9.7 \pm 5.9$	5%	13%
Hierarchical ( $n = 0, \Omega = 0.15$ ) ..	$9.2 \pm 6.0$	6%	14%
Abell clusters .....	$13.2 \pm 6.3$	7%	24%

<sup>a</sup> Column entries give percent of clusters with given  $S2_{\max}$ .

thest galaxy from the adopted center, and the radius encompassing half the total number of galaxies as  $R_{50}$ . In reality, the clusters undoubtedly extend beyond the measured areas presented by Dressler, and thus these values are underestimates of the true  $R_{50}$  and  $R_{100}$ . A comparison of the mean values of  $R_{50}$  and  $R_{100}$  of the observed clusters with those of the simulated clusters showed reasonably good agreement for  $R_{50}$ , although  $R_{100}$  tends to be significantly smaller for the observed clusters. Hence these two tests were applied within regions  $0 < r < R_{50}$  and  $R_{50} < r < R_L$  for the observed clusters, where  $R_L$  is the radius of the largest circle which could be drawn within the measured area. Unfortunately,  $R_L$  often does not extend far beyond  $R_{50}$ . For the density contrast test, however, the entire measured area could be used. The results of these tests are summarized below.

i) *Results from Symmetry Test*

Results from the symmetry test are presented in Figures 5g and 6g. Mean values of  $\beta$  are listed in Table 3. For the region  $0 < r < R_{50}$ , the clusters appear to be quite consistent with few gross deviations from overall symmetry, thus indicating that little significant substructure is present. Similarly, for the region  $R_{50} < r < R_L$ , the observed clusters seem to show little significant substructure, and in fact exhibit a weaker signal of subclustering than the simulated clusters. However, it is highly possible that the observed lack of subclustering in this region may simply result from the fact that  $R_L$  is usually not very large, and hence any substructure which might be present at larger radii would not be included. Nevertheless, within  $R_L$  these results seem to indicate the presence of little, if any, significant subclustering in these observed clusters, or that any substructure which may be present might be quite diffuse. The distribution of values of  $\beta$  found for the observed clusters was then compared with those of the different theoretical scenarios by means of a Kolmogorov-Smirnov (K-S) test. The results of this K-S test are shown in Table 6, in which  $D$  is the maximum value of the absolute difference between the two cumulative distribution functions of  $\beta$  (normalized to range from zero to unity), and  $S$  is the probability of a value of  $D$  greater than the observed one occurring under the null hypothesis that the two distributions are drawn from the same parent distribution, with small values of  $S$  indicating that the two distributions are significantly different. If one imposes a conservative significance level of  $S < 0.01$  for rejection of this null hypothesis, then for the region  $0 < r < R_{50}$ , the distributions of values of  $\beta$  in all the different cosmogonic scenarios are consistent with the observations, while for the region  $R_{50} < r < R_{100}$  none of the different scenarios is consistent with the observed clusters, since the observed clusters exhibit less substructure in this region than do the simulations.

TABLE 6  
RESULTS OF K-S TEST FOR DISTRIBUTIONS OF  $\beta$

SCENARIO VERSUS OBSERVED CLUSTERS	$0 < r < R_{50}$		$R_{50} < r < R_{100}$	
	D	S	D	S
Pancake .....	0.175	0.378	0.461	$4.01 \times 10^{-5}$
Hybrid .....	0.222	0.140	0.708	$1.67 \times 10^{-11}$
Hierarchical ( $n = 0$ ) .....	0.200	0.234	0.647	$1.36 \times 10^{-9}$
Hierarchical ( $n = -1$ ) .....	0.250	0.057	0.611	$3.62 \times 10^{-9}$
Hierarchical ( $n = -2$ ) .....	0.289	0.016	0.590	$1.36 \times 10^{-8}$
Hierarchical ( $n = 0, \Omega = 0.15$ ) ..	0.231	0.114	0.404	$4.85 \times 10^{-4}$

TABLE 7  
RESULTS OF K-S TEST FOR DISTRIBUTIONS OF  $\theta_{\text{hm}}/\theta_{\text{P}}$

SCENARIO VERSUS OBSERVED CLUSTERS	$0 < r < R_{50}$		$R_{50} < r < R_{100}$	
	D	S	D	S
Pancake .....	0.132	0.744	0.207	0.399
Hybrid .....	0.195	0.272	0.211	0.372
Hierarchical ( $n = 0$ ) .....	0.087	0.989	0.218	0.338
Hierarchical ( $n = -1$ ) .....	0.229	0.107	0.174	0.598
Hierarchical ( $n = -2$ ) .....	0.185	0.289	0.227	0.266
Hierarchical ( $n = 0, \Omega = 0.15$ ) ..	0.170	0.429	0.188	0.521

ii) *Results from Angular Separations Test*

The results of the angular separations test for the observed clusters are presented in Figures 7g and 8g. Mean values of this statistic are listed in Table 4. A small signal of subclustering is apparent here, especially at large radii. Comparison of the distribution of values of  $\theta_{\text{hm}}/\theta_{\text{P}}$  for these observations with those of the different scenarios by means of the K-S test (Table 7) shows that there are no statistically significant differences between the distributions found for the observed and simulated clusters for both small and large distances from the cluster center.

iii) *Results from Density Contrast Test*

For the density contrast test, a mean background level of eight galaxies  $\text{deg}^{-2}$  was taken from Dressler (1980b). Results from this test are presented in Figure 9 and in Table 5. It is interesting to note that very few of these clusters possess subclusters which contain a significant fraction of the total system mass. If the same criterion for significant substructure is taken as before, viz.  $S2_{\text{max}} \geq 0.20$ , then only  $\sim 7\%$  of clusters in this sample are found to possess significant subclustering. For a much less stringent criterion of  $S2_{\text{max}} \geq 0.15$  (i.e., only slightly above the expected Poisson noise), the total fraction of such clusters is 24%. Only in one case, A548, does the galaxy distribution consist of essentially two dominant clumps of the sort seen in the simulations by White (1976).

e) *Is There Subclustering beyond Poisson Noise?*

Results from the three statistical tests of subclustering which have been used here indicate the presence of some substructure in both the simulated and observed clusters. However, in terms of the overall cluster mass distribution, the actual amount of such subclustering seems to be quite small. And while there is generally good agreement between the simulations and observations, the observed clusters often seem to have less substructure than the simulated ones, although as discussed in the previous section, this is probably an artifact of the rather small area around each cluster which was observed by Dressler (1980b).

What then could account for the differences in subclustering found here and by Geller and Beers (1982), who claimed to find evidence for much more substructure in the same sample of observational data? Obviously, it must be the different criteria used to assess the significance of substructure. In their study, Geller and Beers used surface number density contour plots based on the galaxy positions given by Dressler to search for substructure in these clusters. These contour plots were generated by counting galaxies in square grid cells, with some smoothing. As a criterion for identifying *significant* substructure, they required that two or more "peaks of interest" lie at least  $3\sigma_R$  above the highest closed contour which surrounds

them, where  $\sigma_R$  is the statistical error in this contour, taken to be the square root of the number of galaxies per cell. However, with this method the significance of any substructure is measured relative to a very local (and arbitrarily chosen) background, which will vary not only from cluster to cluster, but from location to location within a given cluster as well. Because most of their plots are limited by counting statistics, there is a danger than random fluctuations in the local density might produce a false signal of subclustering. Furthermore, although this test examines the density enhancement of subclusters, it says nothing about the actual physical size of any detected substructure; i.e., it does not distinguish between a subcluster containing 5% of the total cluster mass and one containing 50%. Hence, before claiming that some group of galaxies represents a true physical subcluster, one must first test the null hypothesis that these particles are in fact randomly distributed; i.e., is the local number density of galaxies consistent with fluctuations expected in a Poisson distribution?

Following Politzer and Preskill (1986), one can show that in a Poisson distribution of particles having a mean surface density,  $n$ , distributed over a total area,  $A$ , the expected number of clusters per unit area containing  $k$  members within an area,  $a$ , is given by

$$D_k(n, a) = a^{-1} k^2 P_k(n, a), \quad (7)$$

where  $P_k$  is the Poisson probability that a randomly selected region of area  $a$  contains  $k$  particles,

$$P_k(n, a) = (na)^k e^{-na} / (k!). \quad (8)$$

Then the total number of such clusters expected in the area  $A$  is simply  $D_k A$ . Using equation (7), it is possible to show that much of the substructure previously claimed to have been found in Dressler's sample of clusters is in fact consistent with purely random fluctuations. This can be illustrated with specific examples.

Figure 10a shows the galaxy positions given by Dressler for the cluster A754, from which Geller and Beers (1982) claimed that there is a region of significant substructure in the lower right portion of this figure. Examination of their contour plot and Figure 10a shows that this "subcluster" can be easily identified, since it appears fairly isolated; it is indicated by the small box in Figure 10a. The number of galaxies in the claimed subcluster is 9. This represents only  $\sim 6\%$  of the total number of galaxies in this sample, and therefore even if this clump were a genuine physical subcluster, it would seem to be of little consequence in terms of the overall cluster dynamics. One must then ask whether this "subcluster" represents a statistically significant deviation from random fluctuations expected in the galaxy distribution. Obviously the overall distribution of galaxies in A754 is not random, since the cluster is centrally concentrated. However, if the central region is excised, one can then test the hypothesis that the fluctuations in the galaxy distribution in the outer regions (which is much less concentrated) are in fact consistent with Poisson noise. Figure 10a shows a small area which has been cut from the central region of the cluster, leaving 92 galaxies distributed over the remaining area. The smallest box which can be drawn around all nine galaxies in the suspected subcluster has an area  $a \approx 4900 \text{ mm}^2$ . The total area over which the 92 galaxies are distributed is  $A \approx 2.16 \times 10^5 \text{ mm}^2$ , giving a mean surface density  $n \approx 4.27 \times 10^{-4} \text{ galaxies mm}^{-2}$ . Using equation (7), one then calculates that if the galaxies were indeed distributed in a Poisson fashion, one would expect to find  $\sim 0.93$  such

subclusters within this area  $A$ . Hence, the one subcluster which has been found is quite consistent with purely random fluctuations of the galaxy positions. In fact, this procedure actually somewhat underestimates the probability of finding such a subcluster, since choosing the smallest possible box around the subcluster maximizes the local density fluctuation. This same procedure was applied to several other clusters as well. For example, the cluster A119 meets the Geller and Beers criterion for having significant substructure. Their contour plot for this cluster shows several lumps in the galaxy distribution. The three largest clumps are indicated in Figure 10b. Again, the central region shown in this figure has been removed, and then the probabilities of these "subclusters" being simply random fluctuations in the remaining galaxy distribution were calculated. A total of 79 galaxies remain distributed over an area  $A \approx 9.78 \times 10^4 \text{ mm}^2$ , yielding a mean density  $n \approx 8.07 \times 10^{-4} \text{ galaxies mm}^2$ . The clumps labeled "1" and "2" in Figure 10b each contain eight galaxies ( $\sim 7\%$  of the total cluster population), and the smallest box which can be drawn around each is  $a \approx 2070 \text{ mm}$ . Using equation (7), one then calculates the expected number of such clumps in the area  $A$ , assuming a Poisson distribution, to be  $\sim 0.85$ . For the third subcluster, which contains six galaxies within an area  $a \approx 1.48 \times 10^3 \text{ mm}^2$ , one would expect to find, on average,  $\sim 2.9$  such clumps in a random distribution. Thus, the existence of these "subclusters" appears to be consistent with simple random fluctuations. One last example: Geller and Beers contour plot for the cluster A1991 also shows what appears to be a single, isolated subcluster composed of six galaxies (Fig. 10c). However, application of equation (7) shows that the expected probability of finding such a clump is  $\sim 27\%$  in a purely random distribution. Although these calculations are rather crude, they serve to illustrate the point that much of the substructure previously claimed to have been detected in clusters is in fact consistent with the simpler hypothesis of random fluctuations in the local density. Of course, there are many cases where subclusters detected in clusters are in fact quite inconsistent with random fluctuations, thus representing true physical associations. For example, the cluster DC 0317-54 (Fig. 10d) in the Dressler sample contains an isolated group of six galaxies, yet application of equation (7) shows that the number of similar groups expected in a Poisson distribution is only  $\sim 0.04$  (although this subcluster contains only  $\sim 9\%$  of the total population). And one could hardly deny the existence of substructure apparent in the galaxy distribution of clusters such as A548. *Thus, this discussion is not intended to suggest that substructure does not exist within some clusters, but rather that perhaps its occurrence and significance have been overestimated in the past.* The use of density contours for identifying substructure perhaps gives an exaggerated visual impression of just how chaotic the actual galaxy distribution is when the sample contains few galaxies. Certainly the results from the three statistical tests for subclustering which have been used here suggest that significant substructure within clusters is not as common a phenomenon as previously thought and that, when it does occur, the characteristic sizes of these structures are quite small. This means that perhaps clusters are, for the most part, relaxed systems, and thus application of the virial theorem does indeed yield accurate dynamical measures of cluster masses. This question is addressed further in the Appendix.

One additional caveat is warranted: selection effects abound here, in both the observed and simulated clusters. In catalogs of observed galaxy clusters (e.g., Abell 1958), there is most

likely a significant bias caused by the tendency to select nice-looking, regular clusters over those whose appearance is less like the canonical "Coma-like" clusters. Similarly, the "friends-of-friends" technique used in § II to identify clusters in the simulations is likely to miss multicomponent clusters because of their disjointed mass distribution. Just as which criteria one chooses for identifying subclusters largely determines the amount of subclustering one subsequently finds, so too the criteria used for locating and identifying clusters them-

selves may introduce significant biases. Fortunately, however, the aforementioned selection effects in both the simulations and observations are probably very similar, and therefore it seems safe to assume that one really is comparing clusters of a similar nature. Still, as discussed in Paper I, very irregular systems like A1367 are noticeably absent from these simulations, and thus it is possible that none of the cosmogonic scenarios studied here can account for the whole variety of clusters in the real universe.

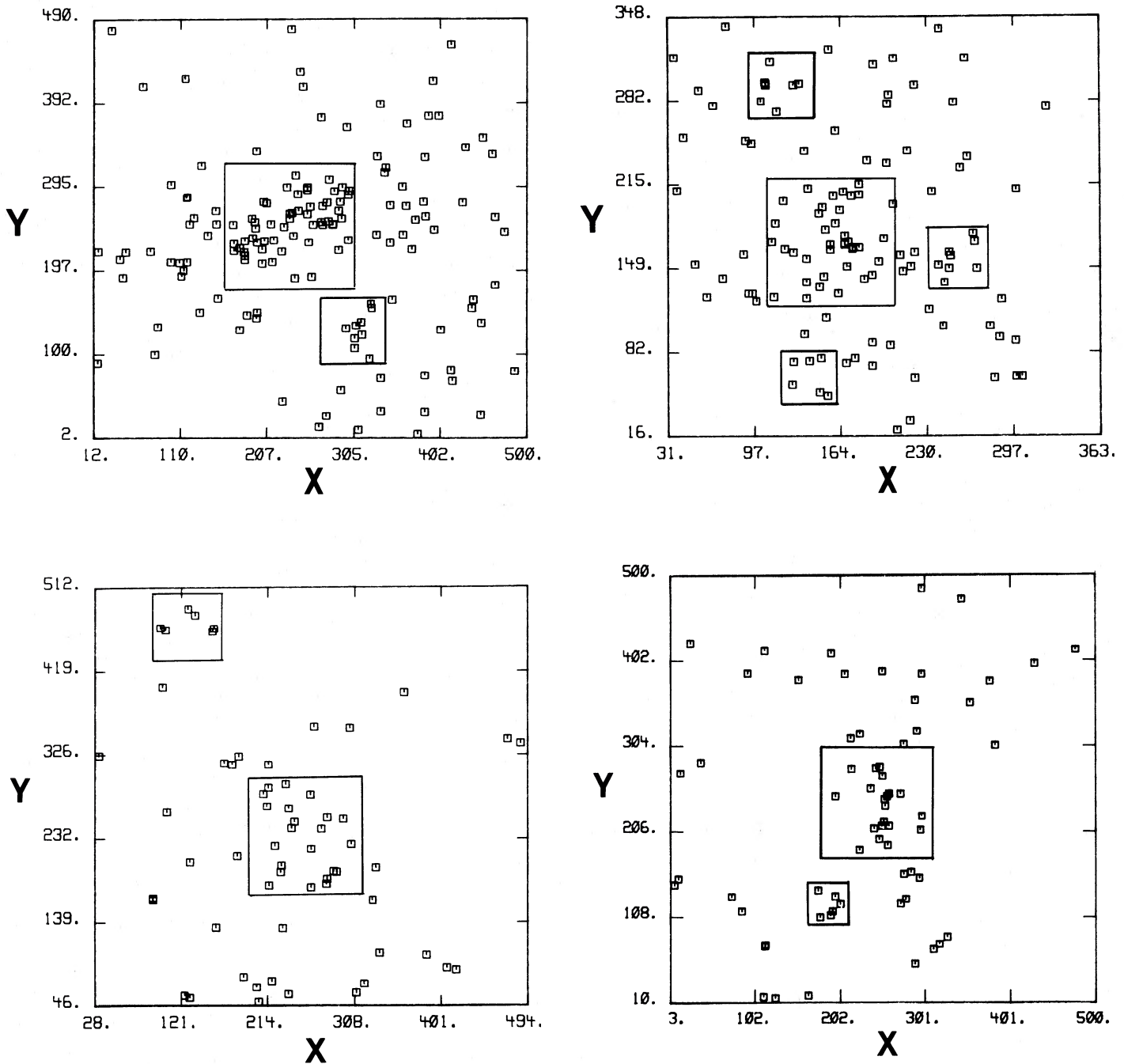


FIG. 10.—Distribution of galaxies from Dressler (1980b) for the following clusters: (a) A754; (b) A119; (c) A1991, (d) DC 0317-54. Small boxes indicate suspected subclusters, and large boxes indicate the central regions which have been removed for calculations discussed in the text.

IV. SMALL-SCALE CLUSTERING IN THE REGIONS  
 SURROUNDING CLUSTERS

Although dynamical effects within clusters appear to quite efficiently obliterate most traces of the cosmological initial conditions which might otherwise have been detectable in the form of subclustering, small-scale clustering in the regions beyond rich clusters might still provide a sensitive test of the different cosmogonies. Visual inspection of Figure 1 suggests that the amount of small-scale clustering present in the environs of rich clusters is indeed a function of the cosmogonic scenario, with those scenarios which originate from fluctuation spectra with significant power on small scales showing a clumpier galaxy distribution in general. As a measure of small-scale clustering in the regions surrounding rich clusters, the symmetry and angular separations tests of § III were applied in the region  $3-8 h^{-1}$  Mpc from the center of each of the simulated clusters. These results are shown in Figures 11 and 12, and summarized in Table 8. It is quite evident that, in most cases, these tests now distinguish very well between the different cosmogonic scenarios. Although the pancake simulations exhibit only a small amount of significant small-scale clustering in the cluster environs, simulations of the hybrid and hierarchical clustering scenarios show a great deal of such clustering in this region. Furthermore, the amount of small-scale clustering detected depends quite sensitively on both the form and slope of the initial power spectrum. A trend of increasing small-scale clustering with distance from the cluster center is clearly indi-

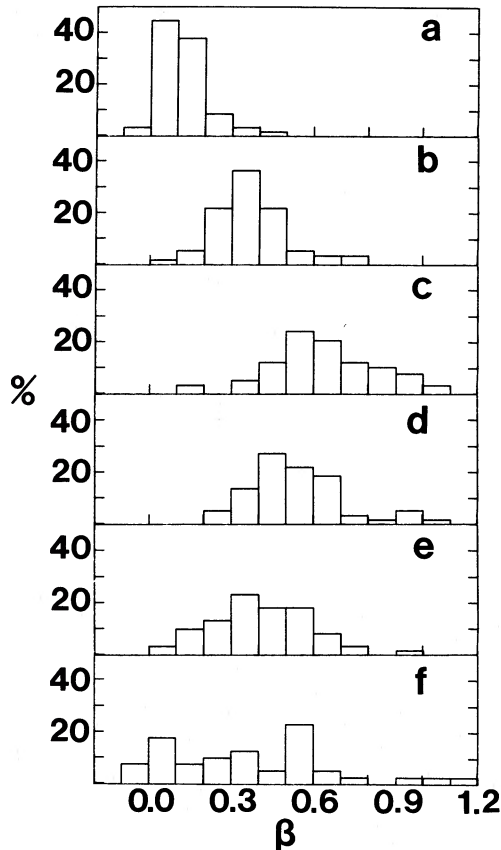


FIG. 11.—Distribution of values of  $\beta$  for the region  $3-8 h^{-1}$  Mpc around each simulated cluster. Labels are the same as in Fig. 5.

TABLE 8  
 RESULTS OF K-S TEST FOR DISTRIBUTIONS OF  $S2_{\max}$

Scenario versus Observed Clusters	D	S
Pancake .....	0.227	0.124
Hybrid .....	0.149	0.585
Hierarchical ( $n = 0$ ) .....	0.212	0.180
Hierarchical ( $n = -1$ ) .....	0.492	$1.81 \times 10^{-6}$
Hierarchical ( $n = -2$ ) .....	0.429	$5.23 \times 10^{-8}$
Hierarchical ( $n = 0, \Omega = 0.15$ ) .....	0.514	$1.26 \times 10^{-6}$

cated in Figure 13, which plots  $\beta(r)$  for three representative scenarios. These results suggest that perhaps a great wealth of information about the initial fluctuations spectrum may come from the region just beyond the confines of rich clusters. Although there are at present few good data available on the distribution of galaxies within several megaparsecs beyond the edges of rich clusters, it would seem that an effort to obtain such data could provide the best means yet for distinguishing between different cosmogonies.

## V. CONCLUSIONS

Substructure and small-scale clustering in and around rich clusters of galaxies formed in different cosmogonic scenarios

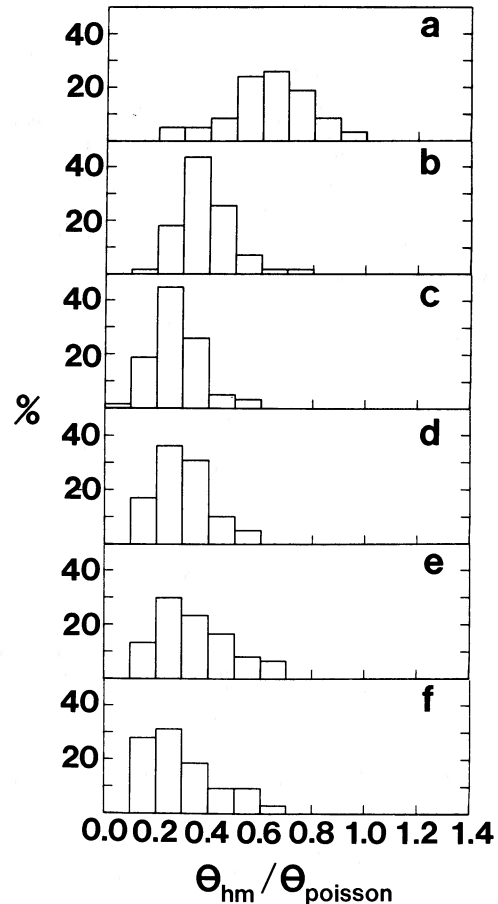


FIG. 12.—Distribution of  $\theta_{hm}/\theta_p$  for the region  $3-8 h^{-1}$  Mpc around each simulated cluster. Labels are the same as in Fig. 5.

TABLE 9  
MEAN VALUES OF STATISTICAL TESTS FOR REGION 3–8  $h^{-1}$  Mpc

Scenario	$\langle\beta\rangle$	$\langle\theta_{\text{hm}}/\theta_p\rangle$
Pancake .....	$0.12 \pm 0.09$	$0.62 \pm 0.16$
Hybrid .....	$0.38 \pm 0.14$	$0.39 \pm 0.11$
Hierarchical ( $n = 0$ ) .....	$0.64 \pm 0.19$	$0.28 \pm 0.10$
Hierarchical ( $n = -1$ ) .....	$0.54 \pm 0.18$	$0.30 \pm 0.10$
Hierarchical ( $n = -2$ ) .....	$0.41 \pm 0.18$	$0.35 \pm 0.15$
Hierarchical ( $n = 0, \Omega = 0.15$ ) .....	$0.38 \pm 0.29$	$0.34 \pm 0.24$

have been studied by means of  $N$ -body simulations and have been compared with available observations. Several new statistical tests for subclustering have been developed and applied to both the simulated and observed clusters (see Table 9). Results from these tests indicate the presence of some substructure in both the simulated and observed clusters. However, in most cases the actual amount of subclustering detected within the inner few megaparsecs is rather small.

For the simulations, the degree of subclustering, especially at greater distances from the cluster center, is found to depend somewhat on the scenario, in the general sense that one might have expected *a priori* on the basis of the initial fluctuation spectrum. Hierarchical clustering scenarios, in which the initial spectrum contains a small-scale component, show a stronger signal of subclustering than the pancake scenario, which has no initial small-scale component. Some slight subclustering does occur in the pancake scenario, originating from nonlinear coupling of perturbations on larger scales. The hybrid scenario, with its lower amplitude small-scale component, yields results intermediate to those of the pancake and hierarchical clustering scenarios. A slight trend can even be seen among the different hierarchical clustering scenarios, with the  $n = 0$  clus-

ters showing a slightly stronger signal of subclustering than the  $n = -2$  case, which is consistent with the former having more power on small scales.

Application of these same tests to Dressler's sample of observed clusters indicates that they also possess little significant substructure. It is argued that previous attempts to quantify the amount of subclustering within clusters have overestimated both its frequency and importance relative to the overall cluster mass distribution. It has been shown that many "subclusters" claimed to have been detected in earlier studies are in fact consistent with Poisson noise. However, it is cautioned that, in general, the "significance" or "insignificance" of subclustering is very subjective, depending greatly on what criteria are chosen for identifying such substructure. Furthermore, selection effects in the cataloging of clusters can introduce serious biases. And ideally one would like to have redshifts for as many cluster members as possible, to confirm the reality of any suspected substructure in velocity space.

Dynamical mass estimates (see Appendix) are consistent with the simulated clusters being in virial equilibrium and, if these simulations provide good models of real clusters, then most rich clusters should be expected to be in a relaxed stage today. Both virial and projected mass estimators are found to yield fairly reliable cluster masses, even in these simulations in which the clusters are generally neither spherical nor isolated, but rather are embedded in larger scale structures which arise in the different cosmogonic scenarios. Hence, it seems that relaxation, which so efficiently erases traces of the initial conditions from the final cluster density and velocity dispersion profiles (Paper I), also succeeds in smearing a significant fraction of the expected differences in the degree of subclustering within rich clusters.

Application of the subclustering tests in regions 3–8  $h^{-1}$

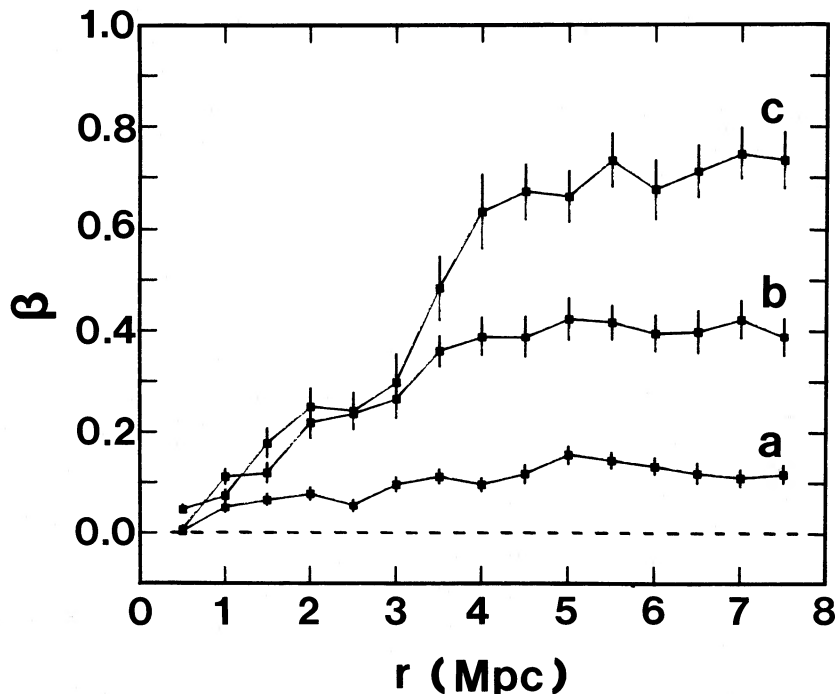


FIG. 13.— $\beta$  as a function of distance from the cluster center for three representative scenarios: (a) pancake; (b) hybrid, and (c)  $n = 0, \Omega = 1$  hierarchical clustering. These values are averages over all clusters.

Mpc from the cluster centers, as a measure of small-scale clustering in the regions surrounding rich clusters, yields results which show a very strong dependence on the cosmogonic scenario from which the clusters arose. The amount of small-scale clustering is found to depend quite sensitively on the amount of power which the initial fluctuation spectrum possesses on small scales, with the greatest degree of such clustering occurring in the  $n = 0$ ,  $\Omega = 1$  hierarchical clustering simulations, and the least found for simulations of the pancake scenario. Similarly, the amount of small-scale clustering is found to be fairly sensitive to the slope of the initial power spectrum in the different hierarchical clustering scenarios. Given the fact that relaxation effects seem to have erased most traces of the initial condition within the inner parts of clusters, it is argued that the regions surrounding rich clusters may provide a

greater wealth of information regarding the initial form of the perturbation spectrum. Differences between the various scenarios might also be reflected in the cluster-cluster and group-group correlation functions, as well as the multiplicity and luminosity functions of bound objects in the universe. It is clear, however, that more and better observations of the galaxy distribution in the few megaparsec regions around rich clusters are needed and should not be prohibitively difficult to obtain.

Many thanks to Sverre Aarseth for kind permission to use his  $N$ -body codes and to Simon White for useful comments. M. J. W. thanks the Weizmann Institute of Science and the Hebrew University of Jerusalem for their generous hospitality during part of this work.

## APPENDIX

### VIRIAL AND PROJECTED MASS ESTIMATES

Ever since Zwicky (1937) attempted to estimate the mass of the Coma cluster from application of the virial theorem, astronomers have continued to use dynamical methods as a means of estimating the masses of groups and clusters of galaxies. Such an approach is based on the fundamental assumptions that clusters are in virial equilibrium, and that the galaxies trace the overall mass distribution within clusters. However, virial theorem mass estimators have at times been criticized as being biased, having large systematic errors, and in general being inefficient from a statistical viewpoint (e.g., Bahcall and Tremaine 1981; Wolf and Bahcall 1972; Rood and Dickel 1979; Heisler, Tremaine, and Bahcall 1985). Checks of dynamical mass estimators almost always consider only isolated, uniform spherical systems, which, while a reasonable assumption for star clusters, might not be valid for observed clusters of galaxies, which are often neither isolated nor spherical. Furthermore, if significant subclustering is indeed a frequent phenomenon in rich clusters, then most clusters must still be in a previrialized stage, and, hence, mass estimates based on the assumption of virial equilibrium are in error (e.g., Geller and Beers 1982; Beers, Geller, and Huchra 1982; Bothun *et al.* 1983). Thus it seems that a brief digression into the issue of dynamical methods of determining the masses of clusters would be of interest here, since the simulations used in this study attempt to treat clusters and their surrounding regions in a more realistic manner, free of *a priori* assumptions regarding the shapes, orientations, mass and velocity distributions, and relative isolation of clusters.

To examine whether or not dynamical mass estimates for the simulated clusters studied here are indeed consistent with them being in a relaxed state, virial and projected mass estimates were compared to the "true" cluster mass,  $M_{\text{true}}$ , as determined by counting all particles within the cluster radius,  $R_{100}$  (see § II). For a self-gravitating system of  $N$  equal-mass particles, an estimate of the virial mass of the system is obtained from

$$M_{\text{vir}} = (3\pi N/2G) \left( \sum_i V_{\text{los}}^2 / \sum_{i<j} r_{ij}^{-1} \right), \quad (\text{A1})$$

where  $G$  is the gravitational constant,  $V_{\text{los}}$  is the line-of-sight velocity of each particle,  $i$  and  $r_{ij}$  is the projected separation between all pairs  $i, j$ . Bahcall and Tremaine (1981) have suggested an alternative method for estimating the mass of spherical systems which is based on moments of the projected mass,

$$M_{\text{proj}} = 24(NG)^{-1} \sum_i (V_{\text{los}}^2 R_i), \quad (\text{A2})$$

where, as before,  $V_{\text{los}}$  is the line-of-sight velocity of particle,  $i$ , and  $R_i$  is its projected radial distance from the cluster center.

Eqs. (A1) and (A2) were used to calculate the virial and projected masses of all clusters in two representative cases, the pancake and  $n = 0$ ,  $\Omega = 1$  hierarchical clustering scenarios. For each cluster, only particles within  $R_{100}$  were used. The values of  $M_{\text{vir}}$  and  $M_{\text{proj}}$  thus determined were then compared to  $M_{\text{true}}$ . Mean values of  $M_{\text{vir}}/M_{\text{true}}$  and  $M_{\text{proj}}/M_{\text{true}}$  from all clusters were

$$\begin{aligned} \langle M_{\text{vir}}/M_{\text{true}} \rangle &= 1.17 \pm 0.23, \\ \langle M_{\text{proj}}/M_{\text{true}} \rangle &= 0.96 \pm 0.33. \end{aligned}$$

Thus it seems that on average both estimators yield reliable measures of the true cluster mass; the variance in these quantities is actually fairly small as well.

Hence, these results suggest that, if these simulated clusters are indeed representative of real ones, then application of the virial theorem yields reliable mass estimates, which is consistent with the clusters being in virial equilibrium. Since the present epoch in these simulations was chosen independently on the basis of the two-point correlation function of the large-scale galaxy distribution, this suggests that most rich clusters should be in a relaxed state today.

## REFERENCES

- Aarseth, S. J. 1984, in *Multiple Time Scales*, ed. J. U. Brackbill and B. I. Cohen (New York: Academic), p. 377.
- Aarseth, S. J., Gott, J. R., and Turner, E. L. 1979, *Ap. J.*, **228**, 664.
- Abell, G. A. 1958, *Ap. J. Suppl.*, **3**, 211.
- Austin, T. B., and Peach, J. V. 1974, *M.N.R.A.S.*, **168**, 591.
- Bahcall, J. N., and Tremaine, S. 1981, *Ap. J.*, **244**, 805.
- Bahcall, N. A. 1971, *A.J.*, **76**, 995.
- Bahcall, N. A., and Soneira, R. M. 1983, *Ap. J.*, **270**, 20.
- Baier, F. W. 1983, *Astr. Nach.*, **304**, 211.
- . 1984, *Astr. Nach.*, **305**, 175.
- Beers, T. C., Geller, M. J., and Huchra, J. P. 1982, *Ap. J.*, **257**, 23.
- Binggeli, B., Tammann, G. A., and Sandage, A. 1987, preprint.
- Bond, J. R., Efstathiou, G., and Silk, J. 1980, *Phys. Rev. Letters*, **45**, 1980.
- Bothun, G. D., Geller, M. J., Beers, T. C., and Huchra, J. P. 1983, *Ap. J.*, **268**, 47.
- Braun, E., and Dekel, A. 1987, in preparation.
- Cavaliere, A., Santangelo, P., Tarquini, G., and Vittorio, N. 1986, *Ap. J.*, **305**, 651.
- Centrella, J., and Melott, A. 1983, *Nature*, **305**, 196.
- Davis, M., Efstathiou, G., Frenk, C. S., and White, S. D. M. 1985, *Ap. J.*, **292**, 371.
- Davis, M., and Peebles, P. J. E. 1983, *Ap. J.*, **267**, 465.
- Dekel, A. 1983, *Ap. J.*, **264**, 373.
- . 1984, *Ap. J.*, **284**, 445.
- Dekel, A., and Aarseth, S. J. 1984, *Ap. J.*, **283**, 1.
- Dekel, A., West, M. J., and Aarseth, S. J. 1984, *Ap. J.*, **279**, 1.
- Doroshkevich, A. G., Khlopov, M., Sunyaev, R., Szalay, A., and Zel'dovich, Y. 1981, *Ann. NY Acad. Sci.*, **375**, 32.
- Doroshkevich, A. G., Shandarin, S. F., and Saar, E. 1978, *M.N.R.A.S.*, **184**, 643.
- Dressler, A. 1978, *Ap. J.*, **226**, 55.
- . 1980a, *Ap. J.*, **236**, 351.
- . 1980b, *Ap. J. Suppl.*, **42**, 565.
- Efstathiou, G., Davis, M., Frenk, C. S., and White, S. D. M. 1985, *Ap. J. Suppl.*, **57**, 241.
- Efstathiou, G., and Eastwood, J. W. 1981, *M.N.R.A.S.*, **194**, 503.
- Fabricant, D., Beers, T. C., Geller, M. J., Gorenstein, P., Huchra, J. P., and Kurtz, M. J. 1986, *Ap. J.*, **308**, 530.
- Fitchett, M. J., and Webster, R. L. 1986, preprint.
- Forman, W., and Jones, C. 1982, *Ann. Rev. Astr. Ap.*, **20**, 547.
- Frenk, C. S., White, S. D. M., and Davis, M. 1983, *Ap. J.*, **271**, 417.
- Frenk, C. S., White, S. D. M., Efstathiou, T., and Davis, M. 1986, preprint.
- Geller, M. J. 1984, *Comments Ap.*, **10**, 47.
- Geller, M. J., and Beers, T. C. 1982, *Pub. A.S.P.*, **94**, 421.
- Gioia, I. M., Geller, M. J., Huchra, J. P., Maccacaro, T., Steiner, J. E., and Stocke, J. 1982, *Ap. J. (Letters)*, **255**, L17.
- Gunn, J. E., and Gott, J. R. 1972, *Ap. J.*, **297**, 16.
- Heisler, J., Tremaine, S., and Bahcall, J. N. 1985, *Ap. J.*, **298**, 8.
- Klypin, A. A., and Shandarin, S. F. 1983, *M.N.R.A.S.*, **204**, 891.
- Mellier, Y., Mazure, A., Mathez, G., Chauvineau, B., and Proust, D. 1987, preprint.
- Melott, A. L. 1983, *Ap. J.*, **264**, 59.
- Miller, R. H. 1983, *Ap. J.*, **270**, 390.
- Oemler, A. 1974, *Ap. J.*, **194**, 1.
- Oemler, A., Schechter, P. L., Shethman, S. A., and Kirshner, R. P. 1987, in preparation.
- Omer, G. C., Page, T. L., and Wilson, A. G. 1965, *A.J.*, **70**, 6.
- Pagels, H. R., and Primack, J. R. 1982, *Phys. Rev. Letters*, **48**, 223.
- Peebles, P. J. E. 1982, *Ap. J.*, **258**, 415.
- Peebles, P. J. E., and Dicke, R. 1968, *Ap. J.*, **154**, 891.
- Politzer, H. D., and Preskill, J. P. 1986, *Phys. Rev. Letters*, **56**, 99.
- Quintana, H., de Souza, R. E., and Arakaki, L. 1986, preprint.
- Rood, H. J., and Dickel, J. R. 1979, *Ap. J.*, **233**, 418.
- Silk, J. 1968, *Ap. J.*, **151**, 459.
- Silk, J., and Turner, M. S. 1986, preprint.
- Struble, M. F., and Rood, H. J. 1981, *Ap. J.*, **251**, 471.
- Turner, M. S., Villumsen, J. V., Vittorio, N., and Silk, J. 1987, preprint.
- West, M. J., Dekel, A., and Oemler, A. 1987a, *Ap. J.*, **316**, 1 (Paper I).
- . 1987b, in preparation (Paper III).
- West, M. J., Oemler, A., and Dekel, A. 1987, in preparation (Paper IV).
- White, S. D. M. 1976, *M.N.R.A.S.*, **177**, 717.
- White, S. D. M., and Rees, M. J. 1978, *M.N.R.A.S.*, **183**, 341.
- Wolf, R. A., and Bahcall, J. N. 1972, *Ap. J.*, **176**, 559.
- Zel'dovich, Ya.B. 1970, *Astr. Ap.*, **5**, 84.
- Zel'dovich, Ya.B., Einasto, J., and Shandarin, S. F. 1982, *Nature*, **300**, 407.
- Zwicky, F. 1937, *Ap. J.*, **86**, 217.

AVISHAI DEKEL: Racah Institute of Physics, Hebrew University of Jerusalem, Jerusalem 91904, Israel

AUGUSTUS OEMLER, JR: Department of Astronomy, Yale University, Box 6666, New Haven, CT 06511

MICHAEL J. WEST: Department of Astronomy, University of Michigan, Dennison Building, Ann Arbor, MI 48109